

STRIVE

Report Series No.62

Health Effects Associated with the Atmospheric Degradation of Polycyclic Aromatic Hydrocarbons

STRIVE

Environmental Protection
Agency Programme

2007-2013

Environmental Protection Agency

The Environmental Protection Agency (EPA) is a statutory body responsible for protecting the environment in Ireland. We regulate and police activities that might otherwise cause pollution. We ensure there is solid information on environmental trends so that necessary actions are taken. Our priorities are protecting the Irish environment and ensuring that development is sustainable.

The EPA is an independent public body established in July 1993 under the Environmental Protection Agency Act, 1992. Its sponsor in Government is the Department of the Environment, Heritage and Local Government.

OUR RESPONSIBILITIES

LICENSING

We license the following to ensure that their emissions do not endanger human health or harm the environment:

- waste facilities (e.g., landfills, incinerators, waste transfer stations);
- large scale industrial activities (e.g., pharmaceutical manufacturing, cement manufacturing, power plants);
- intensive agriculture;
- the contained use and controlled release of Genetically Modified Organisms (GMOs);
- large petrol storage facilities.
- Waste water discharges

NATIONAL ENVIRONMENTAL ENFORCEMENT

- Conducting over 2,000 audits and inspections of EPA licensed facilities every year.
- Overseeing local authorities' environmental protection responsibilities in the areas of - air, noise, waste, waste-water and water quality.
- Working with local authorities and the Gardaí to stamp out illegal waste activity by co-ordinating a national enforcement network, targeting offenders, conducting investigations and overseeing remediation.
- Prosecuting those who flout environmental law and damage the environment as a result of their actions.

MONITORING, ANALYSING AND REPORTING ON THE ENVIRONMENT

- Monitoring air quality and the quality of rivers, lakes, tidal waters and ground waters; measuring water levels and river flows.
- Independent reporting to inform decision making by national and local government.

REGULATING IRELAND'S GREENHOUSE GAS EMISSIONS

- Quantifying Ireland's emissions of greenhouse gases in the context of our Kyoto commitments.
- Implementing the Emissions Trading Directive, involving over 100 companies who are major generators of carbon dioxide in Ireland.

ENVIRONMENTAL RESEARCH AND DEVELOPMENT

- Co-ordinating research on environmental issues (including air and water quality, climate change, biodiversity, environmental technologies).

STRATEGIC ENVIRONMENTAL ASSESSMENT

- Assessing the impact of plans and programmes on the Irish environment (such as waste management and development plans).

ENVIRONMENTAL PLANNING, EDUCATION AND GUIDANCE

- Providing guidance to the public and to industry on various environmental topics (including licence applications, waste prevention and environmental regulations).
- Generating greater environmental awareness (through environmental television programmes and primary and secondary schools' resource packs).

PROACTIVE WASTE MANAGEMENT

- Promoting waste prevention and minimisation projects through the co-ordination of the National Waste Prevention Programme, including input into the implementation of Producer Responsibility Initiatives.
- Enforcing Regulations such as Waste Electrical and Electronic Equipment (WEEE) and Restriction of Hazardous Substances (RoHS) and substances that deplete the ozone layer.
- Developing a National Hazardous Waste Management Plan to prevent and manage hazardous waste.

MANAGEMENT AND STRUCTURE OF THE EPA

The organisation is managed by a full time Board, consisting of a Director General and four Directors.

The work of the EPA is carried out across four offices:

- Office of Climate, Licensing and Resource Use
- Office of Environmental Enforcement
- Office of Environmental Assessment
- Office of Communications and Corporate Services

The EPA is assisted by an Advisory Committee of twelve members who meet several times a year to discuss issues of concern and offer advice to the Board.

EPA STRIVE Programme 2007–2013

Health Effects Associated with the Atmospheric Degradation of Polycyclic Aromatic Hydrocarbons

(2007-FS-EH-3M5)

STRIVE Report

Prepared for the Environmental Protection Agency

by

University College Cork

Authors:

Shouming Zhou and John C. Wenger

ENVIRONMENTAL PROTECTION AGENCY

An Ghníomhaireacht um Chaomhnú Comhshaoil
PO Box 3000, Johnstown Castle, Co. Wexford, Ireland

Telephone: +353 53 916 0600 Fax: +353 53 916 0699

Email: info@epa.ie Website: www.epa.ie

ACKNOWLEDGEMENTS

This report is published as part of the Science, Technology, Research and Innovation for the Environment (STRIVE) Programme 2007–2013. The programme is financed by the Irish Government under the National Development Plan 2007–2013. It is administered on behalf of the Department of the Environment, Heritage and Local Government by the Environmental Protection Agency which has the statutory function of co-ordinating and promoting environmental research.

The assistance received from Dr Robert Healy, Ms Jenny Bell, Mr Yang Chen and Dr Ivan Kourtchev in the present work is greatly acknowledged by the authors.

DISCLAIMER

Although every effort has been made to ensure the accuracy of the material contained in this publication, complete accuracy cannot be guaranteed. Neither the Environmental Protection Agency nor the author(s) accept any responsibility whatsoever for loss or damage occasioned or claimed to have been occasioned, in part or in full, as a consequence of any person acting, or refraining from acting, as a result of a matter contained in this publication. All or part of this publication may be reproduced without further permission, provided the source is acknowledged.

The EPA STRIVE Programme addresses the need for research in Ireland to inform policymakers and other stakeholders on a range of questions in relation to environmental protection. These reports are intended as contributions to the necessary debate on the protection of the environment.

EPA STRIVE PROGRAMME 2007–2013

Published by the Environmental Protection Agency, Ireland

ISBN: 978-1-84095-375-6

Price: Free

Online version

Details of Project Partners

Shouming Zhou*

Department of Chemistry and
Environmental Research Institute
University College Cork
Cork
Ireland
Tel.: +353 21 4901963
Email: s.zhou@ucc.ie

John C. Wenger

Department of Chemistry and
Environmental Research Institute
University College Cork
Cork
Ireland
Tel.: +353 21 4902454
Email: j.wenger@ucc.ie

**Now at:*

Department of Chemistry
University of Toronto
Toronto
ON M5S 3H6
Canada
Tel.: +1 416 9467359
Email: szhou@chem.utoronto.ca
Web: www.chem.utoronto.ca/staff/ABBATT/default.htm

Table of Contents

<u>Acknowledgements</u>	<u>ii</u>
<u>Disclaimer</u>	<u>ii</u>
<u>Details of Project Partners</u>	<u>iii</u>
<u>Executive Summary</u>	<u>vii</u>
<u>1 Introduction</u>	<u>1</u>
<u>1.1 Objectives</u>	<u>1</u>
<u>1.2 Literature Review</u>	<u>1</u>
<u>1.3 Relation of this Work to Legislation</u>	<u>4</u>
<u>2 Experimental Set-Up</u>	<u>5</u>
<u>2.1 Atmospheric Simulation Chambers</u>	<u>5</u>
<u>2.2 Denuder-Filter Sampling System and GC-MS</u>	<u>7</u>
<u>2.3 ATOFMS</u>	<u>8</u>
<u>3 Experiments on Photooxidation of Naphthalene</u>	<u>9</u>
<u>3.1 SOA Yields</u>	<u>9</u>
<u>3.2 Gas- and Particle-Phase Products</u>	<u>16</u>
<u>3.3 SOA Chemical Composition Analysis Using the ATOFMS</u>	<u>19</u>
<u>4 Experiments on Photooxidation of Acenaphthene and Acenaphthylene</u>	<u>21</u>
<u>4.1 Kinetic Studies</u>	<u>21</u>
<u>4.2 Product Studies</u>	<u>28</u>
<u>5 Toxicological Tests</u>	<u>35</u>
<u>5.1 Experimental</u>	<u>35</u>
<u>5.2 Results and Discussion</u>	<u>35</u>
<u>6 Conclusions and Recommendations</u>	<u>37</u>
<u>References</u>	<u>38</u>
<u>Acronyms</u>	<u>41</u>

Executive Summary

Polycyclic aromatic hydrocarbons (PAHs) are major air pollutants produced from combustion processes. They can be chemically transformed in the atmosphere to generate a range of secondary pollutants, including ozone and secondary organic aerosol (SOA) which are known to have an adverse effect on human health. In this project, a comprehensive programme of laboratory studies was carried out on the atmospheric degradation of three PAHs:

1. Naphthalene;
2. Acenaphthene; and
3. Acenaphthylene.

The principal findings of the research are:

- Naphthalene produces SOA in higher yields than most monoaromatic compounds, confirming that naphthalene is likely to be a significant source of SOA in urban areas.
- The atmospheric degradation of naphthalene produces a range of products (some known to be toxic) that are partitioned between the gas and particle phases. The chemical composition of the particles continuously changes as a result of oxidation.

- New information has been obtained on the atmospheric degradation of acenaphthene and acenaphthylene. The provision of accurate kinetic data has reduced the level of uncertainty over the atmospheric lifetimes of these compounds and new reaction pathways have been proposed for their atmospheric degradation.
- Biochemical assays showed that the SOA generated from all three PAHs can produce reactive oxygen species and thus affect cellular function. Further tests, including those using cell-based assays, are required to investigate the reproducibility of the experiments and the possible correlation of quinone concentrations with toxicity.

The type of information generated in this project can be used to assess the impact of PAH emissions on air quality and human health. Exposure to fine particulate matter is one of the primary threats to human health in Ireland and worldwide. A clear understanding of the sources and composition of fine particulate matter is therefore required to provide policy makers and legislators with the necessary information to reduce ambient levels in order to meet European Union directives on air quality.

1 Introduction

Polycyclic aromatic hydrocarbons (PAHs) are ubiquitous air pollutants that are released into the atmosphere as a by-product of combustion processes. PAHs can be chemically transformed in the lower atmosphere to produce a range of oxidised organic compounds and other pollutants such as ozone (O₃) and secondary organic aerosol (SOA) (Finlayson-Pitts and Pitts, 2000). Epidemiological studies have established that exposure to this type of air pollution is associated with damaging effects on the respiratory and cardiovascular systems, and can lead to asthma, oxidative stress, health deterioration and even death (Dockery et al., 1993).

Secondary organic aerosol is responsible for between 30% and 80% of the total mass of ambient fine particulate matter (PM) (Finlayson-Pitts and Pitts, 2000). The major anthropogenic source of SOA in urban areas is believed to be aromatic hydrocarbons, which are present in automobile fuels and are used as solvents (Bolton et al., 2000). As a result, research is currently being performed on the characterisation of SOA produced from aromatic hydrocarbons such as toluene, xylenes and trimethylbenzene. However, significant amounts of PAHs are also released into urban areas from automobile emissions and from the combustion of fossil fuels for home heating. Since gas-phase PAHs react in an analogous manner to monocyclic aromatic compounds, they may also be expected to make a significant contribution to ambient SOA. Despite their importance, relatively little is known about the atmospheric chemistry of even the simplest PAHs, mainly because of the variety and complexity of the reaction products. Indeed, although the atmospheric degradation of naphthalene, the simplest PAH, has been investigated on several occasions (Bolton et al., 2000), the reported product yields are not in agreement and, on average, only around 50% of the reacted naphthalene is accounted for. Furthermore, the atmospheric degradation of naphthalene and other gas-phase PAHs, including acenaphthene and acenaphthylene, is known to produce SOA, but the yield and chemical composition of the aerosol is not

well characterised. Therefore, further investigations into the atmospheric degradation of gas-phase PAHs and their role in the health effects associated with exposure to PM are clearly needed.

1.1 Objectives

The overall goal of this research project was to investigate the health effects associated with the atmospheric degradation of polycyclic aromatic hydrocarbons. Three key objectives were identified:

1. Determination of the yield of SOA produced from the atmospheric degradation of PAHs;
2. Identification and quantification of the major gas- and particle-phase degradation products; and
3. Investigations into the toxicological effects of the SOA produced from PAHs.

1.2 Literature Review

In the atmosphere, PAHs containing two and three rings are found predominantly in the gas phase, whilst those containing six or more rings principally adsorb to particles. Polycyclic aromatic hydrocarbons with four or five rings are found in both phases (Finlayson-Pitts and Pitts, 2000). The chemical structures of some of the most important PAHs detected in the gas phase at urban locations around the world are shown in [Fig. 1.1](#). Typical mixing ratios for naphthalene, the simplest PAH, are in the range of 0.05–0.20 parts per billion (ppbV) in European cities. There are no reported gas-phase measurements of naphthalene or other PAHs in ambient air in Ireland.

A comprehensive review of the atmospheric degradation of PAHs was performed by Calvert et al. (2002). The degradation of PAHs in the atmosphere is mainly initiated via gas-phase reaction with the hydroxyl (OH) radical, although reaction with O₃ and nitrate (NO₃) radicals may also be possible for certain species (Calvert et al., 2002). The OH-radical-initiated oxidation of naphthalene has been investigated on several occasions (Atkinson et al., 1987; Bunce et al.,

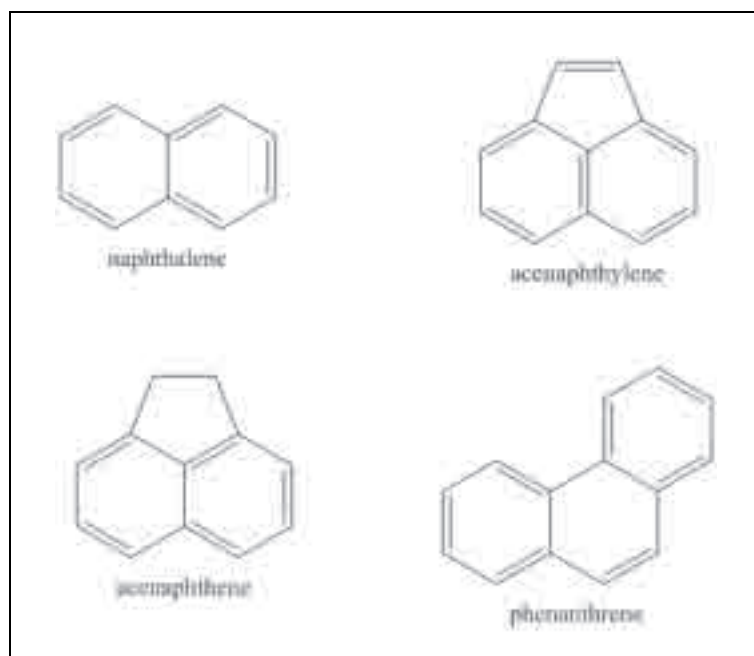


Figure 1.1. Chemical structures of some of the most abundant polycyclic aromatic hydrocarbons detected in ambient urban air.

1997; Sasaki et al., 1997; Bolton et al., 2000) and leads to the formation of a range of oxidation products including naphthols, nitro-naphthalenes and aromatic carbonyls (Fig. 1.2). In the recent work of Wang et al. (2007a), a number of other dicarbonyl compounds (including glyoxal) were also identified as reaction products of naphthalene oxidation. However, the reported product yields from different research groups are not in agreement and, on average, only around 50% of the reacted naphthalene is accounted for. As a result, a detailed mechanism of the OH-radical-initiated oxidation of naphthalene is not well understood. In addition, the atmospheric degradation of naphthalene is known to produce SOA, but the yield and chemical composition of the aerosol have not been determined. The need for further investigations into the mechanisms for the degradation of naphthalene and its oxidation products is clearly evident and has been acknowledged by international experts in the most recent review of the subject (Calvert et al., 2002).

The subsequent chemistry of the naphthalene oxidation products has been the subject of only one recent study – Wang et al. (2006) investigated the photolysis and OH-radical-initiated oxidation of

phthalaldehyde, and other related compounds. It is clear that very little is known about the second-generation chemistry relating to the atmospheric oxidation of naphthalene.

As mentioned above, other PAHs, e.g. acenaphthene, acenaphthylene and phenanthrene, are also emitted into the atmosphere from a variety of incomplete combustion sources such as diesel exhaust (Cousins and Mackay, 2001). However, the atmospheric degradation of these PAHs has received considerably less attention than that afforded to naphthalene. Research published in the peer-reviewed literature has largely focused on the kinetics of the atmospheric oxidation of these PAHs (Biermann et al., 1985; Atkinson and Aschmann, 1988; Atkinson and Arey, 1994; Kwok et al., 1994; Brubaker and Hites, 1998; Bernhard and Simonich, 2000; Calvert et al., 2002; Reisen and Arey, 2002; Lee et al., 2003; Annathula et al., 2007). Product and mechanistic studies are sparse (Atkinson and Arey, 1994), with the reported formation of 9,10-phenanthrenequinone from the atmospheric reaction of phenanthrene (Wang et al., 2007b) being the only significant reported work on this topic. The formation yields and chemical composition of SOA arising from the gas-phase oxidation of acenaphthene,

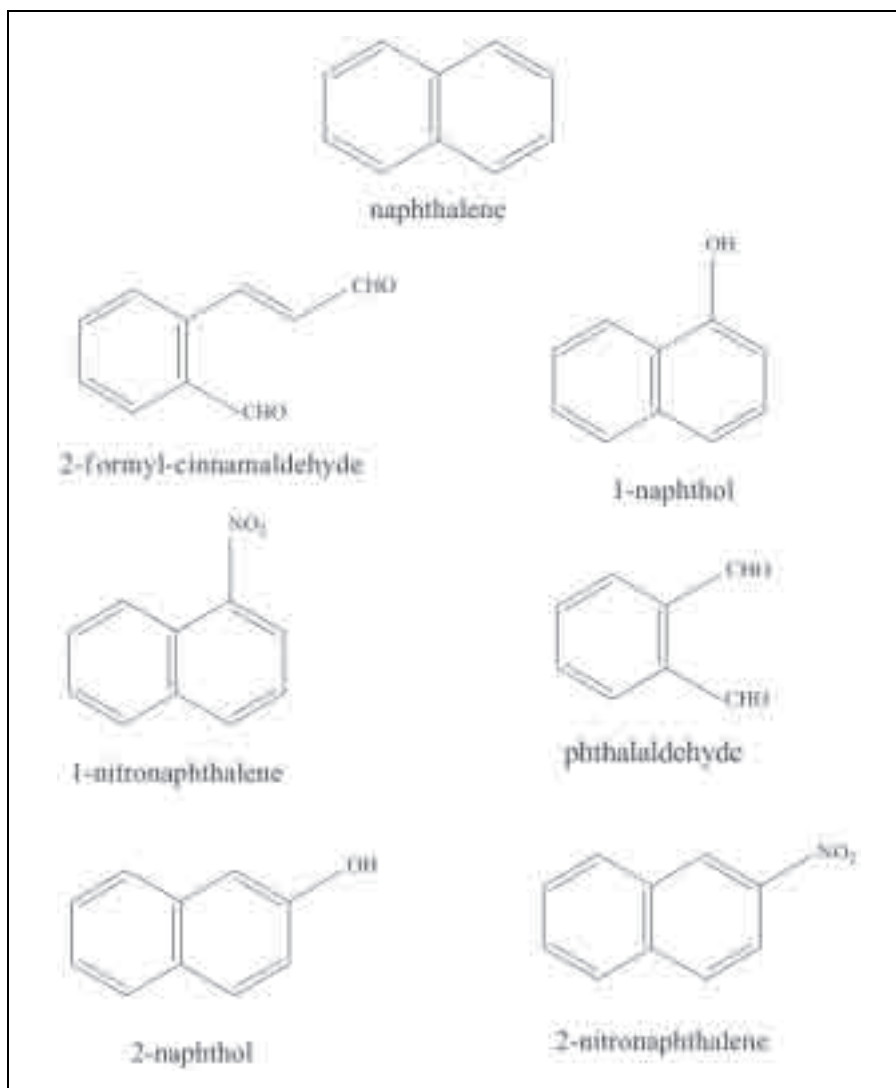


Figure 1.2. The major atmospheric oxidation products of naphthalene.

acenaphthylene and phenanthrene have not been studied yet.

The environmental fate and impact of PAHs and their oxidation products have been the subject of several reviews (Atkinson and Arey, 1994; Bolton et al., 2000; Calvert et al., 2002; Srogi, 2007), with the most recent article published in 2007 (Srogi, 2007). The group of compounds that appears to have the largest impact on human health is the quinones, which are first-generation oxidation products of PAHs.

The chemical structures of two quinones regularly detected in ambient air (mainly in the particulate phase) are shown in [Fig. 1.3](#). Many of the toxic effects associated with quinones are attributed to their ability

to form reactive oxygen species (ROS) and to cause oxidative stress (Atkinson and Arey, 1994; Bolton et al., 2000; Srogi, 2007). Reactive oxygen species are formed intracellularly by reducing agents such as nicotinamide adenine dinucleotide (NADH) and nicotinamide adenine dinucleotide phosphate (NADPH) aided by electron transfer chemicals such as quinones (Bolton et al., 2000).

Because of their potential toxicological significance, the formation of quinones in the photooxidation of PAHs needs to be determined and the toxicological tests need to be performed. This information is expected to be especially important in calculating the health risk associated with exposure to fine PM generated from combustion sources.

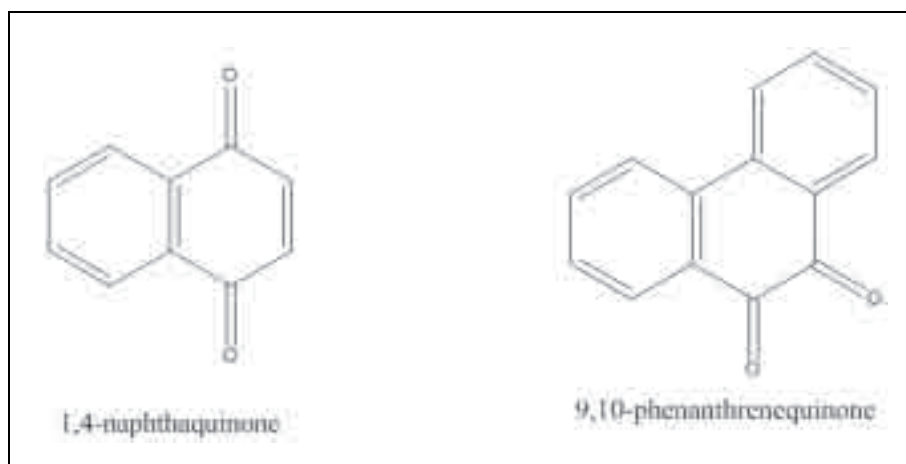


Figure 1.3. Chemical structures of two quinones regularly identified in ambient particulate matter.

1.3 Relation of this Work to Legislation

The research programme presented in this proposal will provide important information on the atmospheric degradation of a number of PAHs and the associated health effects. The information can be used to assess the impact of PAH emissions on air quality and will also prove useful to scientists investigating the health effects of photochemical smog and SOA. The proposed work is of high national relevance as indicated in Environmental Protection Agency (EPA) annual reports on the state of the environment, which regularly identify “nitrogen dioxide and fine particulate

matter as the primary threat to the quality of air in Ireland”.

A clear understanding of the sources and composition of atmospheric particles is required to determine the health effects of exposure to PM and also to provide environmental policy makers and legislators with the necessary information to help reduce ambient levels, particularly in urban areas, in order to meet targets laid down in European Union directives on air quality. Further research into understanding the composition and health effects of ambient PM is therefore of top priority.

2 Experimental Set-Up

2.1 Atmospheric Simulation Chambers

The research work started with studies on the atmospheric degradation of naphthalene, the simplest of the PAHs. At the first stage of the research, some test experiments were performed to develop the best sampling and analytical conditions for naphthalene. A detailed series of experiments on the OH-radical-initiated oxidation of naphthalene was performed in a 6,500-l atmospheric simulation chamber (Fig. 2.1).

The chamber is a cuboid made of FEP (fluorine–ethene–propene) Teflon foil and is surrounded by 12 Philips TL05 (40 W) lamps ($\lambda_{\text{max}} = 360 \text{ nm}$) and 12

Philips TL12 (40 W) lamps ($\lambda_{\text{max}} = 310 \text{ nm}$). A detailed description of the chamber and its operation for SOA formation experiments can be found elsewhere (Termime et al., 2007; Healy et al., 2008). The chamber was flushed with purified air and humidified by flowing purified air through the headspace of an impinger containing heated deionised (Milli-Q) water. Temperature and relative humidity (RH) were measured using a dewpoint meter (Vaisala DM70). A PAH, i.e. naphthalene, acenaphthene or acenaphthylene, was introduced through a heated impinger and its concentration was monitored using a gas chromatograph (Varian CP3800) equipped with a



Figure 2.1. The 6,500-l atmospheric simulation chamber at University College Cork.

flame ionisation detector (FID). A known volume of nitric oxide (NO) (98%, Aldrich Chemical Company) was added to a small glass bulb and flushed directly into the chamber with dry purified air or nitrous acid (HONO) was generated by adding a 1% sodium nitrite (NaNO_2) aqueous solution dropwise into a flask containing 30% sulfuric acid, which was introduced into the chamber. Nitric oxide and nitrogen oxides (NO_x) concentrations were measured with a chemiluminescence NO_x analyser (Thermo model 42i). Ozone concentration was measured with an ultraviolet (UV) photometric O_3 analyser (Thermo model 49i). The formation and evolution of particles in the range 10–470 nm was monitored using a scanning mobility particle sizer (SMPS, TSI Model 3034).

After being introduced into the chamber, the reactants and HONO/ NO_x were kept in the dark for at least 30 min to allow for mixing. The photooxidation of PAHs was initiated by switching on the TL05 lamps in the chamber. Due to the absence of a cooling system, the temperature in the chamber increased from approximately 293 to 305 K within the first hour of the reactions. The lamps were turned off when SOA volume concentrations had reached a maximum.

Kinetic studies on the atmospheric degradation of acenaphthene and acenaphthylene and the analysis of SOA chemical composition for photooxidation of naphthalene were performed in a 3,910-l simulation chamber (Fig. 2.2).

The chamber is made of FEP Teflon foil and is surrounded by 12 Philips TL05 (40 W) lamps ($\lambda_{\text{max}} = 360$ nm) and 18 Philips TL12 (40 W) lamps ($\lambda_{\text{max}} = 310$ nm). A white-type mirror system mounted internally within the chamber, and coupled to a Fourier Transform Infrared (FTIR) spectrometer equipped with a global as the infrared (IR) source and a liquid-nitrogen-cooled mercury–cadmium–tellurium (MCT) detector, enables in situ IR monitoring of the reactants. The chamber was flushed with purified air and humidified by flowing purified air through the headspace of an impinger containing heated deionised (Milli-Q) water. Temperature and RH were measured using a dewpoint meter (Vaisala DM70). As in the 6,500-l reactor, NO and NO_x concentrations were measured with a chemiluminescence NO_x analyser (Thermo model 42i) and O_3 concentration was measured with a UV photometric O_3 analyser (Thermo model 49i). The formation and evolution of particles in the range 10–470 nm was monitored using an SMPS (TSI Model 3080).



Figure 2.2. The 3,910-l reaction chamber at University College Cork.

2.2 Denuder-Filter Sampling System and GC-MS

Determining the chemical compositions of both the gas- and particulate-phase products from the photooxidation of PAHs was performed by using a denuder-filter sampling technique to collect the gas- and particulate-phase products coupled with gas chromatography–mass spectrometry (GC-MS) analysis. The denuder (Fig. 2.3), which consisted of five concentric glass tubes, was coated with absorbent XAD-4 resin. After collecting the products for 30 min at

~10 l/min gas flow, the denuder and filter were extracted with methanol and analysed using GC-MS.

A Varian Saturn 2000 ion-trap GC-MS, which consisted of a Varian CP 3800 gas chromatograph and a fused silica capillary column (5% diphenyl, 95% dimethyl-polysiloxane, 0.25 µm film thickness, 0.25 mm internal diameter, and 30 m in length), was used to analyse the products (Fig. 2.4). The ion source was operated using both chemical ionisation (CI) and electron ionisation (EI) modes.

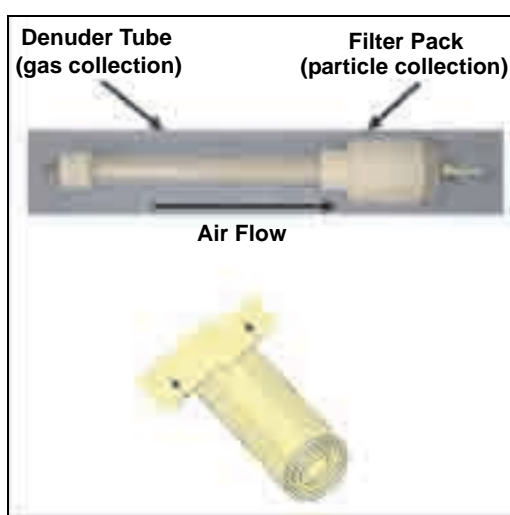


Figure 2.3. Denuder coupled with filter pack used in chemical composition analysis.



Figure 2.4. The gas chromatograph–mass spectrometer used in the experimental work.

2.3 ATOFMS

The Aerosol Time-of-Flight Mass Spectrometer (ATOFMS) is a commercially available instrument (TSI 3800, MN, USA) (Fig. 2.5) designed to sample and analyse the composition of single aerosol particles in real time.

Particle-laden air is sampled and accelerated into a sizing region where the aerodynamic diameter of individual particles is determined. The particles pass into a bipolar time-of-flight mass spectrometer and are desorbed and ionised using a UV laser operating at 266 nm. The resulting positive and negative ions generated from a single aerosol particle are detected by the spectrometer, thus generating two complete

mass spectra from each individual particle. The ATOFMS is portable and can measure particles in the size range 30–3,000 nm and record mass spectra of species up to 800 Da. It is routinely used for analysing ambient atmospheric aerosols. The successful application of the ATOFMS in probing the chemical composition of SOA produced in simulation chamber experiments was demonstrated for the first time by Gross et al. (2006), who performed measurements of the SOA generated from the photooxidation of 1,3,5-trimethylbenzene and α -pinene. This study showed that the ATOFMS is not only capable of the online detection of oligomers in SOA, but also that the chemical evolution of these species can be followed in real time.



Figure 2.5. The Aerosol Time-of-Flight Mass Spectrometer (TSI 3800) used in the experimental work at University College Cork.

3 Experiments on Photooxidation of Naphthalene

3.1 SOA Yields

A series of 18 experiments was performed on the photooxidation of naphthalene in the presence of NO_x . Details of the experimental conditions and associated parameters are summarised in [Table 3.1](#). The concentration–time profiles were qualitatively similar in all experiments, with the decay of hydrocarbon accompanied by conversion of NO to nitrogen dioxide

(NO_2) and the subsequent formation of O_3 , as shown in [Fig. 3.1](#).

Secondary organic aerosol formation was observed after 24–83 min, depending on experimental conditions. Following nucleation, the particles continued to increase in size and mass due to condensation and coagulation before reaching a maximum concentration after 180–300 min. It should

Table 3.1. Experimental conditions and results.

Experiment	RH (%)	HC_0^1 (ppbV)	NO_x^2 (ppbV)	HC_0/NO_x (ppb/ppb)	ΔHC^3 ($\mu\text{g}/\text{m}^3$)	M_0^4 ($\mu\text{g}/\text{m}^3$)	SOA yield (%) ⁵	Nucleation time (min)	$[\text{OH}]^6$
RH0_1	0.2	1,070	520	1.95	2,198	285.5	13.0	68	2.3
RH0_2	0.6	1,040	240	4.35	1,807	330.1	18.3	27	2.3
RH0_3	0.8	1,084	250	4.34	2,118	379.6	17.9	48	2.2
RH0_4	0.7	1,081	510	2.13	2,135	237.3	11.1	81	2.4
RH0_5	0.8	830	690	1.20	1,310	136	10.3	57	2.1
RH0_6	0.8	602	145	4.15	1,470	248.5	16.9	60	2.8
RH0_7	1.9	508	500	1.02	954	63.4	6.64	83	2.2
RH0_8	1.3	611	202	3.02	1,444	230.8	16.0	72	2.8
RH25_1	25.1	585	470	1.24	1,022	118.6	11.6	33	2.4
RH25_2	25.3	593	540	1.01	926	103.8	11.2	36	2.2
RH25_3	25.1	532	520	1.02	1055	97.2	9.23	48	2.4
RH25_4	25.5	611	344	1.78	1,408	229.4	15.5	36	2.7
RH25_5	25.6	626	517	1.21	1,168	155	13.3	39	2.3
RH25_6	25.3	699	556	1.26	1,745	271.3	15.5	33	2.6
RH50_1	50.3	629	590	1.07	1,276	218.5	17.1	24	3.2
RH50_2	49.2	514	496	1.04	1,061	159.4	15.0	27	3.0
RH50_3	50.6	602	370	1.63	1,287	206.9	16.1	33	3.1
RH50_4	51.0	705	410	1.72	1,651	309.7	18.8	27	3.2

¹Initial hydrocarbon (naphthalene) mixing ratio.

²Initial nitrogen oxides (NO_x) mixing ratio.

³Amount of parent hydrocarbon reacted, corrected for dilution and dark-wall loss.

⁴Secondary organic aerosol (SOA) mass concentration, determined at the time of measured maximum particle volume concentration, corrected for wall loss, assuming a density of $1.4 \text{ g}/\text{cm}^3$.

⁵Calculated from $M_0/\Delta\text{HC}$.

⁶Average OH radical concentration (in $10^5 \text{ molecules}/\text{cm}^3$), determined from the measured decay of naphthalene using a rate coefficient of $2.3 \times 10^{-11} \text{ cm}^3/\text{molecule}/\text{s}$ (Calvert et al., 2002).

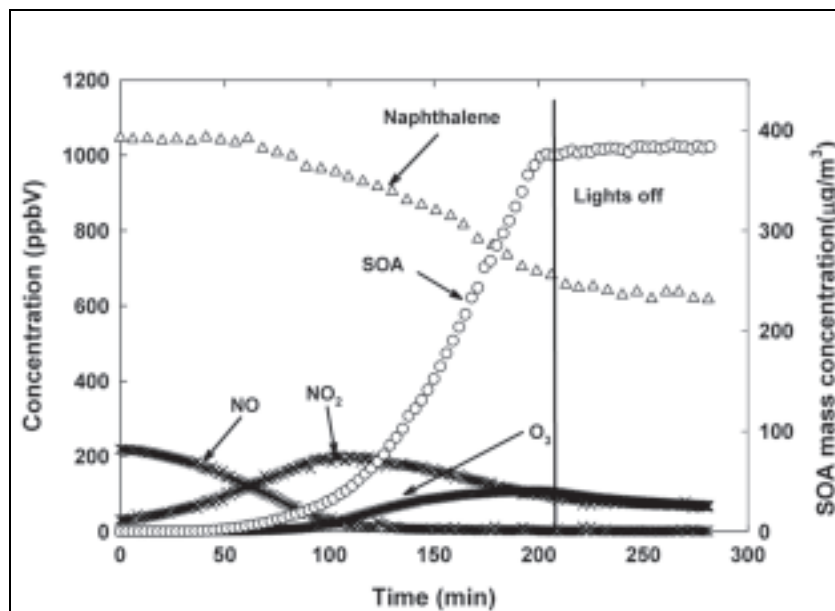


Figure 3.1. Typical concentration–time profile for the photooxidation of naphthalene.

be noted that the temperature increase in the chamber only occurred within the first hour of the reactions and that much of the SOA formation and growth took place whilst the temperature was relatively constant at 303–305 K. One particularly interesting feature of the concentration–time profiles is that SOA nucleation started even while the NO concentration was as high as 150–200 ppbV. This is in sharp contrast to the classical photooxidation experiments performed on monocyclic aromatics, where SOA formation and growth is observed only when the NO concentration approaches zero (Sasaki et al., 1997; Wang et al., 2006). It was initially proposed that the primary oxidation products of the organic peroxy radical (RO_2) + NO reactions are too volatile to undergo condensation and that SOA formation is only observed at low NO concentrations when the RO_2 + hydroperoxy radical (HO_2) reactions begin to dominate and generate a range of lower volatility products such as peroxyhemiacetals and organic hydroperoxides (Johnson et al., 2004, 2005). However, Ng et al. (2007) subsequently showed that products of the RO_2 + NO reactions are in fact condensable, but contribute to aerosol mass only when the oxidation reactions are fast, e.g. when direct injection of HONO is used as the OH radical source. Under classical photooxidation conditions, such as those performed in this work, it was proposed that the primary oxidation products of RO_2 +

NO reactions are formed too slowly and competing processes such as further gas-phase reaction or wall deposition are favoured over nucleation and condensation. Although this explanation holds for the monocyclic aromatic hydrocarbons, the observed formation of SOA at high NO_x levels in this work clearly indicates that the primary products of RO_2 + NO reactions during the photooxidation of naphthalene are able to undergo nucleation and condensation even when the reaction is relatively slow. Naphthalene oxidation products, such as nitronaphthalene, 2-formyl-cinnamaldehyde, phthalaldehyde and naphthol (Bunce et al., 1997; Sasaki et al., 1997; Calvert et al., 2002; Atkinson and Arey, 2007), have higher molecular weight and thus lower volatility than their monocyclic counterparts and are thus more likely to undergo condensation. As the reaction progresses, these products may also contribute to SOA via further reaction with OH radicals, O_3 , and NO_3 radicals.

3.1.1 Effects of hydrocarbon to NO_x ratio on SOA yield

The SOA formation yield, Y , is defined as the fraction of the hydrocarbon (ΔHC) ($\mu\text{g}/\text{m}^3$) that is converted into organic aerosol:

$$Y = \frac{M_0}{\Delta\text{HC}} \quad \text{Eqn 3.1}$$

where, M_0 ($\mu\text{g}/\text{m}^3$) is the total organic aerosol mass concentration. The yield of SOA produced in each experiment was determined from the values of reacted naphthalene (ΔHC) and M_0 at the point where the maximum particle concentration was observed. Both ΔHC and M_0 were corrected for wall losses by applying first-order loss rates obtained from measuring the dark decay of naphthalene and the particles at the end of each experiment. M_0 was calculated from the volume concentration of SOA by assuming a density of $1.4 \text{ g}/\text{cm}^3$ (Chan et al., 2009). The calculated yields are listed in Table 3.1 and show a range of values that depend on the initial concentrations of naphthalene and NO_x , as well as RH.

The effect of the hydrocarbon to NO_x ratio (HC_0/NO_x) can be seen by comparing the results from the experiments performed under dry ($\text{RH} < 2\%$) conditions, RH0_1 to RH0_8. As indicated in Table 3.1, higher SOA mass yields were obtained when HC_0/NO_x was higher. This effect has also been observed for monocyclic aromatic hydrocarbons (Cocker et al., 2001; Ng et al., 2007; Song et al., 2007a) and has generally been attributed to differences in peroxy radical chemistry under high and low NO_x conditions, as outlined above. However, the same explanation cannot be applied here because

SOA formation always occurred when high amounts of NO_x were present. Plots of M_0 vs time reveal that the time required for the formation of particles (nucleation time) depends on HC_0/NO_x and humidity (Fig. 3.2).

Comparison of the nucleation times for the experiments performed under dry conditions (Table 3.1) clearly shows that the nucleation time becomes shorter as HC_0/NO_x is increased. A similar effect was also apparent in the photooxidation of *m*-xylene under high NO_x conditions in the absence of seed aerosol (Song et al., 2005). Shorter nucleation times would be expected to promote condensation of the oxidation products, thus increasing the rate and yield of aerosol formation. One possible reason for shorter nucleation times is a higher photooxidation rate. The average OH radical concentration during each experiment was determined from the measured decay of naphthalene using a rate coefficient of $2.3 \times 10^{-11} \text{ cm}^3/\text{molecule}/\text{s}$ (Calvert et al., 2002) and is listed in Table 3.1. For experiments RH0_7, RH25_3 and RH50_2 (data shown in Fig. 3.2), which were performed at similar HC_0/NO_x levels but different RH conditions, the reduction in nucleation time does appear to be linked with higher OH concentrations, as discussed below. However, for the experiments performed under dry conditions, the OH levels are very similar and show no

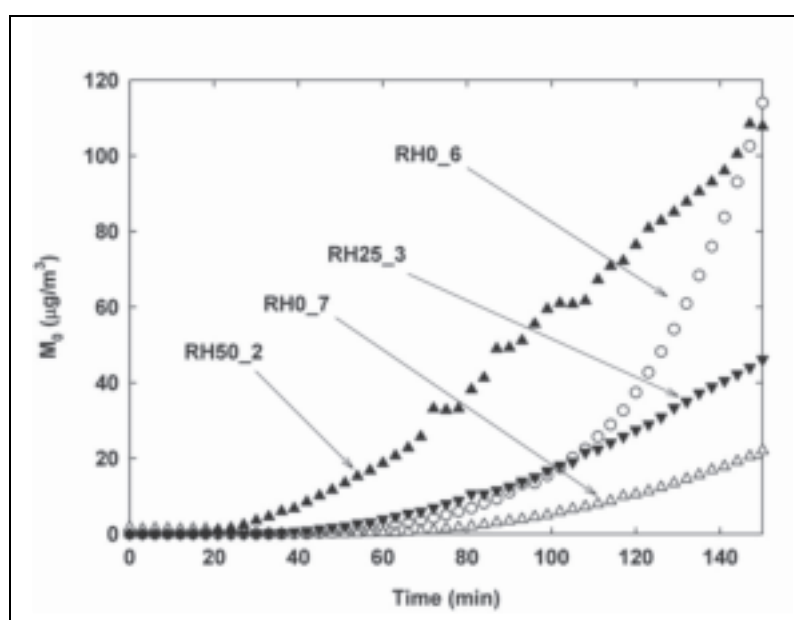


Figure 3.2. Secondary organic aerosol mass concentration (M_0) as a function of time for selected experiments to show the effect of initial conditions on the time required for particle nucleation.

clear relationship with nucleation time or SOA yield. This implies that another factor is responsible for the reduction in nucleation time as HC_0/NO_x is increased. Additional experiments, e.g. where species in the gas and aerosol phase are monitored in real time, may help to explain this observation.

The SOA yield (Y) obtained for each experiment is plotted against M_0 in [Fig. 3.3](#).

The data points clearly fall into four categories, which reflect the different initial reaction conditions. For each category, a yield curve was produced by fitting the data points to the gas-particle partitioning model proposed by Odum et al. (1996, 1997):

$$Y = M_0 \sum_{i=1}^n \left(\frac{\alpha_i K_i}{1 + M_0 K_i} \right) \quad \text{Eqn 3.2}$$

where α_i is the mass-based stoichiometric yield of the oxidation product i , K_i ($m^3/\mu g$) is the partitioning coefficient and n is the number of product species. Best-fit yield curves were generated using one-product and two-product models, but the two-product model did not improve the quality of the fit. Previous studies performed on aromatic compounds under similar conditions have generally found that a two-product

model provides the best fit to the experimental data (Odum et al., 1997; Song et al., 2005), indicating that two types of products with different volatility are responsible for SOA formation. However, Henry et al. (2008) recently showed that SOA yields from the photooxidation of cresols are best described by a one-product model. The cresols, like naphthalene, mainly generate ring-retaining oxidation products with lower volatility than those produced by the alkylbenzenes (Calvert et al., 2002) and it is thus not surprising to find that products with higher volatility do not appear to be involved in SOA formation in either system. The values of α and K determined using the one-product model are shown in [Table 3.2](#).

Under dry conditions, a larger value of α is obtained when HC_0/NO_x is higher, while the K values are similar, suggesting that the same types of products partition into the particle phase. As shown in [Table 3.2](#), an increase in RH leads to a larger α value, indicating a higher yield of aerosol-forming products.

In the only previous investigation of the SOA yields from naphthalene photooxidation, Chan et al. (2009) reported yields in the range 19–30% under high NO_x conditions at an RH of 5–8%. Although these values are somewhat higher than those obtained in the

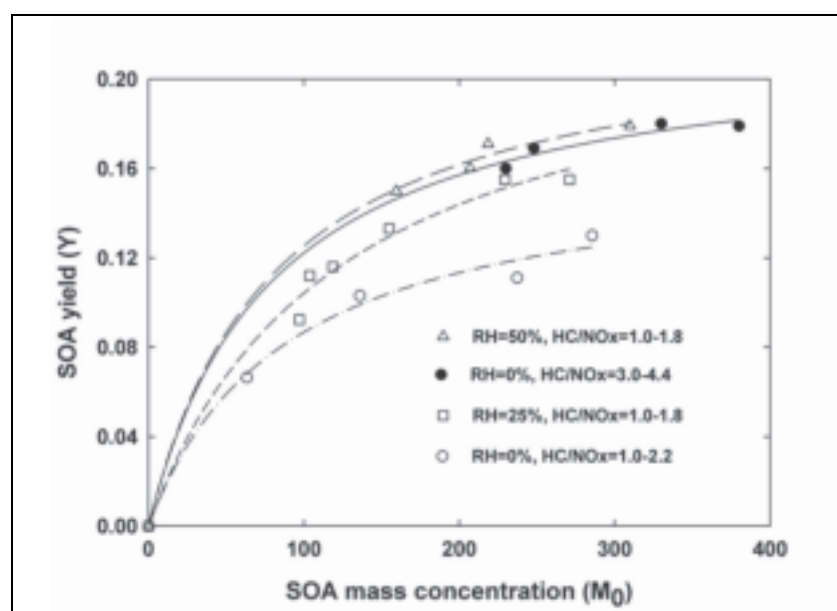


Figure 3.3. Yield curves for the photooxidation of naphthalene as a function of the ratio of hydrocarbon to nitrogen oxides (HC_0/NO_x) and relative humidity (RH). SOA, secondary organic aerosol.

Table 3.2. Aerosol yield parameters obtained from the best fit of the experimental data to the gas-particle partitioning model by assuming one product partitioning.

Data group	α_1	K_1 ($\text{m}^3/\mu\text{g}$)	Average OH (10^6 molecules/ cm^3)
RH < 2%, $\text{HC}_0/\text{NO}_x = 1.0\text{--}2.2$	0.1645	0.0111	2.1–2.4
RH < 2%, $\text{HC}_0/\text{NO}_x = 3.0\text{--}4.4$	0.2246	0.0116	2.2–2.8
RH = 25%, $\text{HC}_0/\text{NO}_x = 1.0\text{--}1.8$	0.2324	0.0081	2.2–2.7
RH = 50%, $\text{HC}_0/\text{NO}_x = 1.0\text{--}1.8$	0.2595	0.0084	3.0–3.2

OH, hydroxyl radical; RH, relative humidity; HC_0/NO_x , ratio of hydrocarbon to nitrogen oxides.

present work, there are a number of significant differences in the experimental conditions employed in the two studies. Chan et al. employed the direct injection of HONO as the OH radical source, which is known to produce higher concentrations of OH than in classical photooxidation experiments (Ng et al., 2007). This results in the faster decay of reactants and generates higher SOA yields. The presence of seed aerosol in the experiments performed by Chan et al. (2009) was also expected to increase the yield of SOA via enhanced partitioning of the oxidation products. Chan et al. used a two-product model to generate yield curves for naphthalene, but found that a one-product model provided the best fit for SOA production from methylnaphthalenes. The SOA yields for naphthalene were about three times those for monocyclic aromatics under similar photooxidation conditions, thus confirming the potential of naphthalene as an important source of SOA in urban areas. Similarly, the yields obtained from this work are also higher than those for toluene (Hurley et al., 2001) and the xylenes (Song et al., 2005, 2007a) under classical photooxidation conditions.

3.1.2 Effect of RH on SOA yields

The effect of RH on SOA yields was investigated by performing a series of experiments in which initial water concentration was varied while the HC_0/NO_x ratios were maintained in a similar range, i.e. $\text{HC}_0/\text{NO}_x = 1\text{--}2$. As shown in [Table 3.1](#), it is clear that there is an increase in the SOA yields at higher RH. The best-fit yield curves obtained at 25% and 50% RH are shown in [Fig. 3.3](#) and the corresponding SOA yield parameters are listed in [Table 3.2](#). The value of α increases by a factor of 1.5 over the RH range 0–50%;

however, the value of K does not change significantly, indicating that products with similar volatility (probably the same products) are formed in all cases.

Several studies have been performed on the effect of water vapour on SOA formation during the photooxidation of monocyclic aromatic hydrocarbons (Kleindienst et al., 1999; Edney et al., 2000; Cocker et al., 2001). Kleindienst et al. (1999) studied the hygroscopicity of SOA formed from the photooxidation of toluene, *p*-xylene, and 1,3,5-trimethylbenzene in the presence of dry ammonium sulfate seed aerosol and determined that water uptake by the organic fraction was negligible. Edney et al. (2000) reported similar findings for SOA produced from toluene photooxidation and two other independent studies have shown that SOA yields from *m*-xylene and 1,3,5-trimethylbenzene are largely unaffected by the presence of gas-phase water up to an RH of 50% (Cocker et al., 2001; Baltensperger et al., 2005). As a result, the uptake of water is unlikely to account for the increase in yields with RH observed in this study.

The effect of RH on SOA yields from the classical photooxidation of *p*-xylene, was recently reported by Healy et al. (2009). The SOA yields increased by a factor of approximately two over the RH range 5–75% and were found to correlate with OH concentration. In classical photooxidation experiments, OH is initially produced from the photolysis of HONO generated from the heterogeneous reaction of gas-phase NO_2 with water at the chamber walls (Finlayson-Pitts et al., 2003) or from an unidentified source that is strongly dependent on humidity (Rohrer et al., 2005). Healy et al. (2009) therefore proposed that an increase in RH results in higher levels of HONO formation in the

chamber which leads to increased OH concentration, a faster hydrocarbon decay rate and higher aerosol mass yields. Inspection of the data reported in [Table 3.1](#) indicates that the same effect is also apparent in the photooxidation of naphthalene. The SOA yields and average OH concentrations determined for experiments in each of the four categories (listed in [Table 3.2](#)) rise as the RH is increased to 50%. A plot of the average OH concentrations vs α , which effectively represents the maximum SOA yield, is shown in [Fig. 3.4](#).

A good correlation is observed, which indicates that the SOA yield is strongly influenced by OH radical concentration and thus the photooxidation rate of naphthalene. A similar 'rate effect' has also been observed in other studies when factors that affect the OH concentration, e.g. type of precursor (Song et al., 2007a,b), light intensity and wavelength (Warren et al., 2008), are varied. As expected, the faster decay of naphthalene at higher RH results in shorter nucleation times ([Table 3.1](#)). This promotes the condensation of oxidation products and increases the rate and yield of aerosol formation, as shown in [Fig. 3.2](#) for experiments RH0_7, RH25_3 and RH50_2, which were performed at similar HC_0/NO_x levels but different RH conditions.

[Figure 3.5](#) shows typical SOA growth curves for experiments performed under each of the four different sets of initial conditions.

The two experiments performed under dry conditions (RH0_3 and RH0_4) clearly show that SOA formation is delayed and only occurs after a certain amount of naphthalene has reacted. This so-called 'induction period' is a characteristic feature of classical photooxidation experiments on monocyclic aromatic hydrocarbons (Ng et al., 2007; Song et al., 2007a) and is strongly dependent on the HC_0/NO_x ratio – shorter induction periods are observed when HC_0/NO_x is higher. Comparison of the growth curves for experiments RH0_3 ($HC_0/NO_x = 4.34$) and RH0_4 ($HC_0/NO_x = 2.13$) confirms that the same effect is apparent for naphthalene oxidation under dry conditions. It is interesting to note, however, that an induction period is not observed in experiments at higher RH.

Ng et al. (2007) showed that the induction period disappears when experiments are performed under very low NO_x levels ($RO_2 + HO_2$ reactions dominate) or when hydrocarbon photooxidation in the presence of NO_x occurs at a faster rate, e.g. when direct injection of HONO is used as the OH radical source. In the

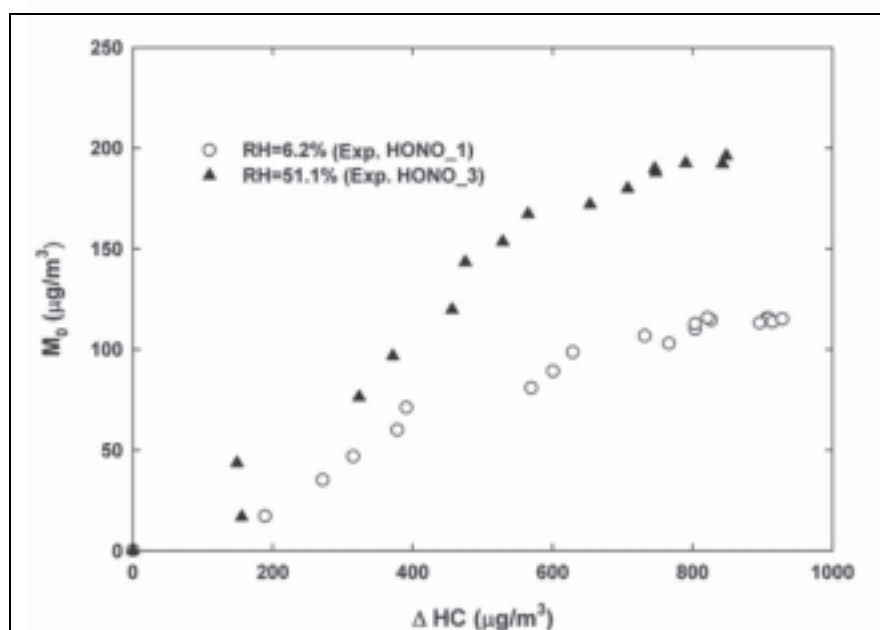


Figure 3.4. Growth curves for nitrous acid (HONO) experiments under different relative humidity (RH) conditions. M_0 , the total organic aerosol mass concentration; HC, hydrocarbon.

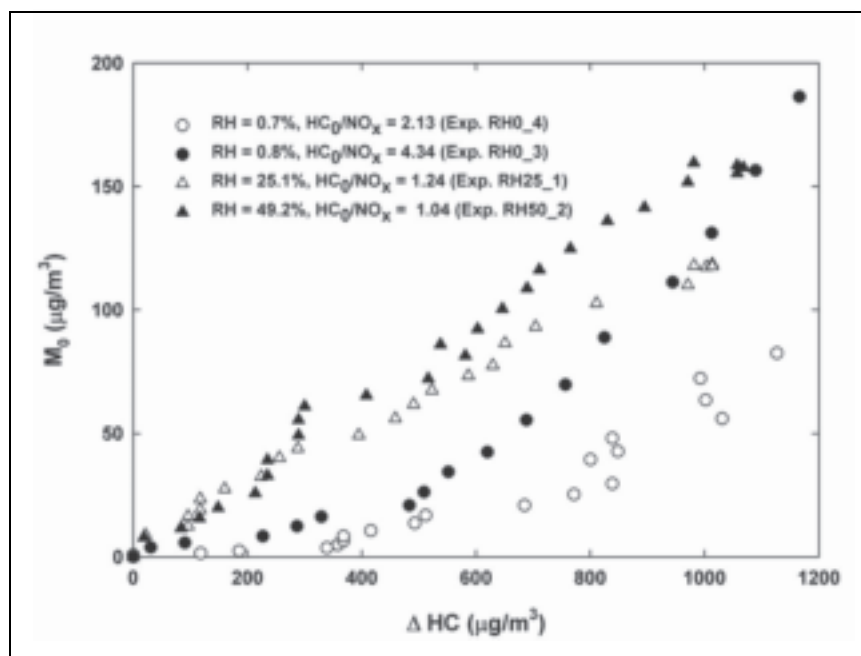


Figure 3.5. Growth curves for secondary organic aerosol formation under different initial experimental conditions. M_0 , the total organic aerosol mass concentration; RH, relative humidity; HC_0/NO_x , ratio of hydrocarbon to nitrogen oxides; HC, hydrocarbon.

experiments performed in this work, SOA formation was observed even in the presence of high levels of NO_x and it therefore seems most likely that the absence of an induction period in the experiments performed at RH = 25% and 50% is due to a faster oxidation rate compared with dry conditions. The absence of an induction period implies that the nucleation time should be close to zero. However, as shown in [Table 3.1](#), nucleation times for experiments at 25% and 50% RH are in the range 24–45 min. This apparent discrepancy may be explained by the changes in naphthalene concentrations observed during the experiments. As shown in [Fig. 3.1](#), there is a delay in the decay of naphthalene, indicating that the initial concentration of OH radicals is not sufficient to cause appreciable loss of the hydrocarbon. However, as time progresses, the naphthalene begins to react, and in the experiments performed at RH = 25% and 50%, SOA formation subsequently occurs within 3–6 min. This observation suggests that although HONO may initially be present in the reaction system due to the dark heterogeneous reaction of NO_2 with water at the chamber walls (Finlayson-Pitts et al., 2003), a larger photolytic source of HONO is required to fully initiate the photooxidation process (Rohrer et al.,

2005). Further evidence for the importance of a photolytic source of HONO has recently been provided by Metzger et al. (2008) who proposed that a reaction involving the light-induced conversion of NO_2 to HONO at the chamber walls is responsible for much higher levels of HONO than those generated by dark reactions.

The aerosol growth curves for naphthalene reported by Chan et al. (2009) also show an induction period when experiments were performed under high NO_x conditions using HONO as the OH precursor. The experiments were performed under relatively dry conditions (RH ~8%) and the effect of RH was not investigated. Chan et al. (2009) proposed that the induction period may be due to the formation of relatively volatile photooxidation products from the $RO_2 + NO$ reactions. This does not concur with the data obtained in this study, where the observed formation of SOA at high NO_x levels indicates that the primary products of $RO_2 + NO$ reactions during the photooxidation of naphthalene are able to undergo nucleation and condensation. Thus, it seems that the very different reaction conditions employed in the two studies may have influenced the yield and volatility of

some of the first-generation oxidation products and, in turn, the rate of aerosol formation and growth. There are three important differences of note. Firstly, the photooxidation rates employed in the present study are 4–15 times larger than those used by Chan et al. (2009), indicative of a significant possible difference in the 'rate effect'. Secondly, the HC₀/NO_x ratio employed by Chan et al. (in the range 0.024–0.042) was much lower than in the present work and, as shown in [Fig. 3.4](#), would be expected to result in a larger 'induction period'. Finally, there are different levels of NO₂ present in the reaction systems. The initial OH-naphthalene adduct can react with O₂ to form peroxy radicals or NO₂ to produce nitronaphthalenes (Sasaki et al., 1997; Calvert et al., 2002; Atkinson and Arey, 2007; Nishino et al., 2008), which are relatively non-volatile species likely to influence SOA formation. The relative rates of the competing reactions for the OH-naphthalene adduct depend on the concentration of NO₂ and Nishino et al. (2008) recently reported that the reaction of the OH-naphthalene adduct with O₂ and NO₂ was comparable at an NO₂ mixing ratio of 60 ppbV. Chan et al. (2009) used NO₂ mixing ratios in the range 50–100 ppbV in their experiments but did not observe nitronaphthalene as an oxidation product. The NO₂ levels in the present work typically reached a maximum of 150–250 ppbV, which are slightly more favourable conditions for nitronaphthalene formation. The possible formation of non-volatile nitronaphthalenes may therefore help to explain, at least in part, some of the differences observed between the two studies.

The results reported in the present work and by Chan et al. (2009) indicate that naphthalene is a potentially large source of SOA in urban areas and should be included in atmospheric SOA models. This work also highlights the need for further detailed investigations of SOA formation from naphthalene and other PAHs under a wide variety of reaction conditions. Detailed information on the chemical composition of the SOA would also be of great value in elucidating mechanistic details of SOA formation and growth.

3.2 Gas- and Particle-Phase Products

Gas- and particle-phase products resulting from the OH-radical-initiated oxidation of naphthalene were

produced at 298 ± 5 K in purified air at atmospheric pressure in a 6,500-l rectangular FEP Teflon chamber ([Fig. 2.1](#)). The photolysis of HONO under TL05 lamps was used as the OH radical precursor:



Nitrous acid was synthesised by adding a 1% NaNO₂ aqueous solution dropwise into a flask containing 30% sulfuric acid. The initial concentration of acenaphthene was 1–2 ppm. The decay of acenaphthene was determined by an online GC-FID. A denuder-filter sampling technique was employed to collect the gas- and particulate-phase products ([Fig. 2.3](#)) using a flow rate of 10 l/min for 30 min. The contents of the denuder and filter were extracted with methanol and derivatised using *O*-(2,3,4,5,6-pentafluorobenzyl)-hydroxylamine (PFBHA) and *N,O*-Bis(trimethylsilyl)trifluoroacetamide (BSTFA) to aid the detection of carbonyls and OH-group-containing products, respectively ([Fig. 3.6](#)).

After derivatisation, the products were analysed by GC-MS. The GC conditions for PFBHA-derivatised products were: initial oven temperature 60°C, held for 1 min, then ramped from 60°C to 100°C at 5°C/min, from 100°C to 280°C at 10°C/min and from 280°C to 310°C at 30°C/min, held for 5 min. Helium was used as carrier gas at 1 ml/min. The MS was operated at EI and in full scan mode over a mass range of 60–650. The GC conditions for BSTFA-derivatised products were: initial oven temperature 50°C, held for 5 min, then ramped from 50°C to 200°C at 3.5°C/min, from 200°C to 310°C at 30°C/min, held for 2 min. Helium was used as carrier gas at 1.2 ml/min.

3.2.1 PFBHA-derivatised products

[Figures 3.7](#) and [3.8](#) show the products identified in both the gas and particulate phases for the photooxidation of naphthalene using PFBHA and BSTFA derivatisation techniques, respectively.

From PFBHA derivatisation, the following species were detected: benzaldehyde, nitronaphthalene, 1,4-naphthoquinone, glyoxal and 1-naphthol. From BSTFA derivatisation, the following products were identified: 1-naphthol, 2-naphthol, phthalic acid, 2-formylcinnamic acid. It is clear from [Fig. 3.8](#) that several major peaks in the chromatogram have not been identified yet. It should be noted that 2-formylcinnamaldehyde and

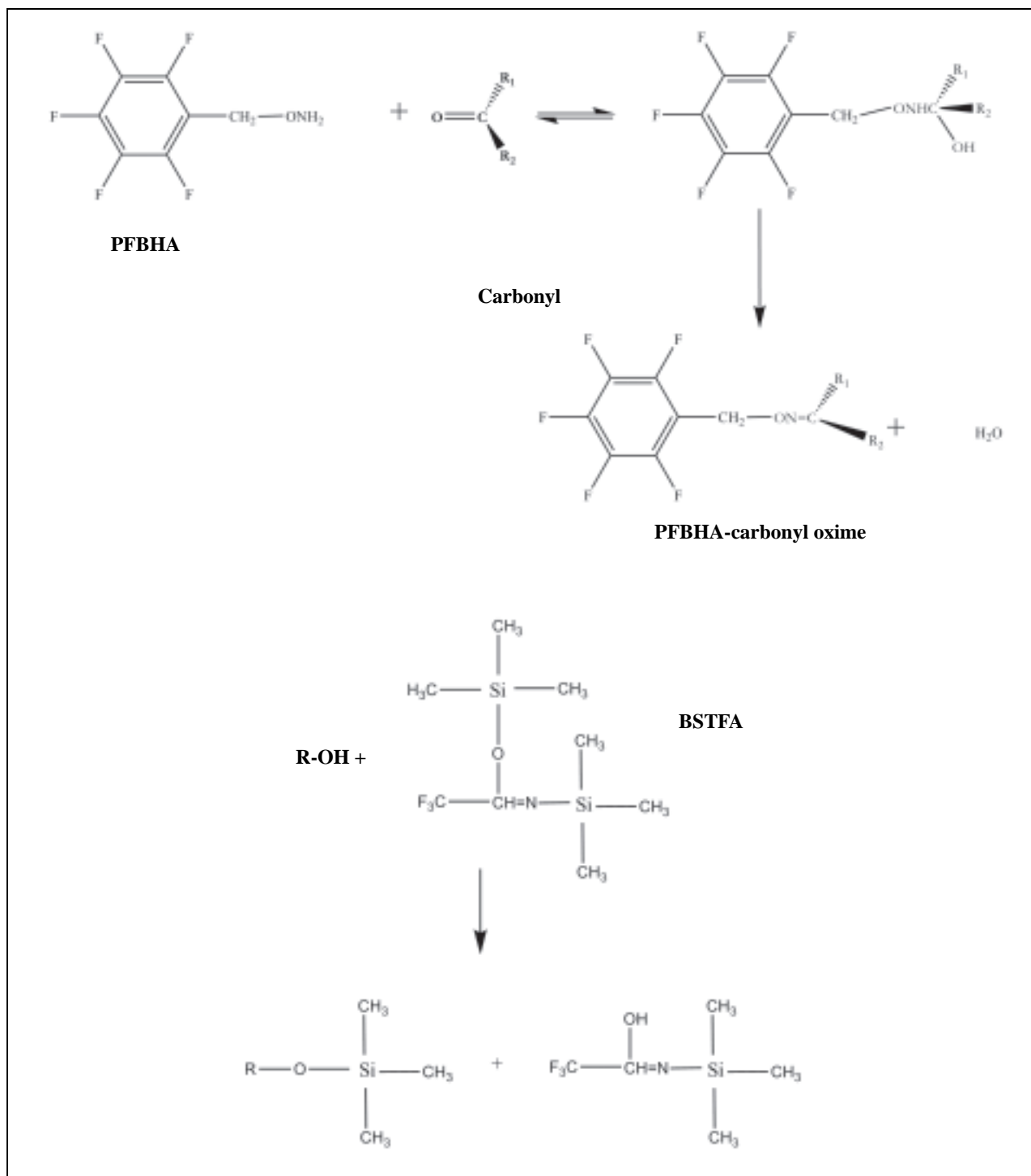


Figure 3.6. Reaction of using O-(2,3,4,5,6-pentafluorobenzyl)-hydroxylamine (PFBHA) with carbonyls (top) and N,O-Bis(trimethylsilyl)trifluoro acetamide (BSTFA) with hydroxyl (OH)-group-containing products (bottom).

phthalialdehyde have been reported as major products in the photooxidation of naphthalene in previous studies; however, the formation of these two products has not been observed in the present work.

Instead, the formation of 2-formylcinnamic acid and phthalic acid was observed and they should be formed from further oxidation of 2-formylcinnamaldehyde and phthalialdehyde, respectively.

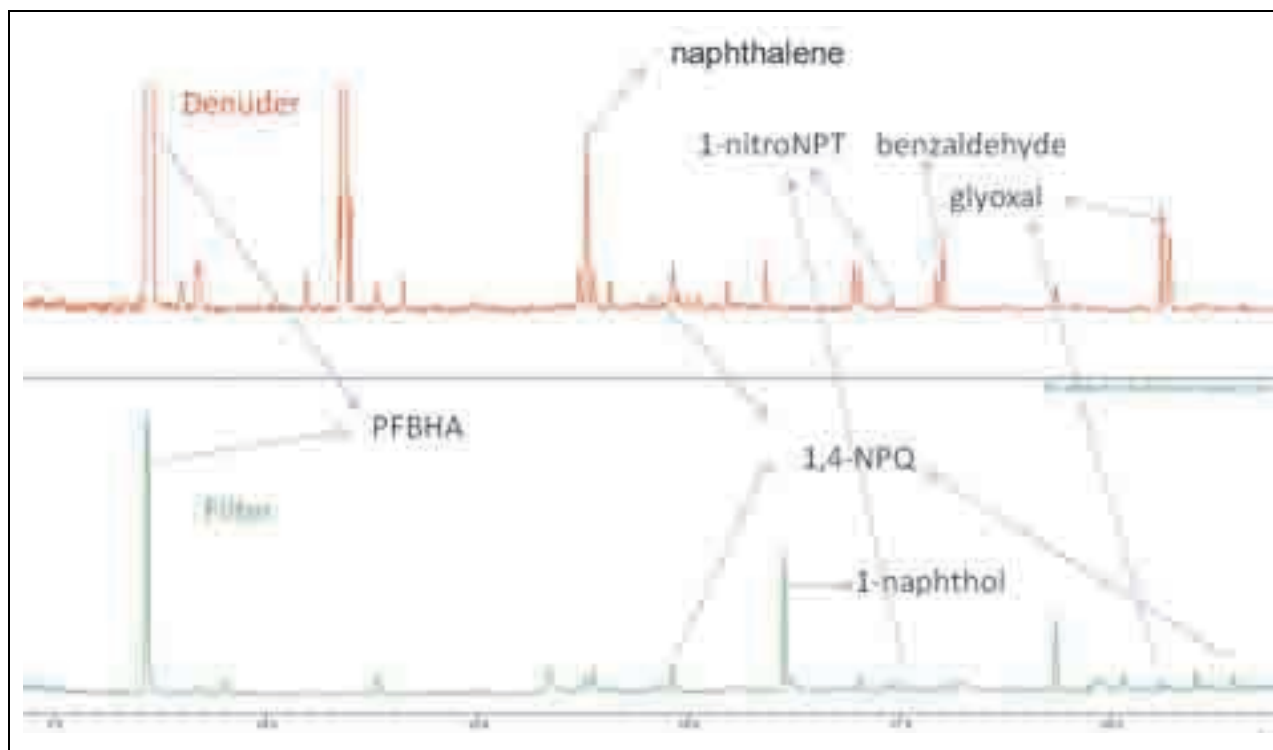


Figure 3.7. Products identified from photooxidation of naphthalene using *O*-(2,3,4,5,6-pentafluorobenzyl)-hydroxylamine (PFBHA) derivatisation. NPT, nitrophenylthiocyanate; 1,4-NPQ, 1,4-naphthoquinone.

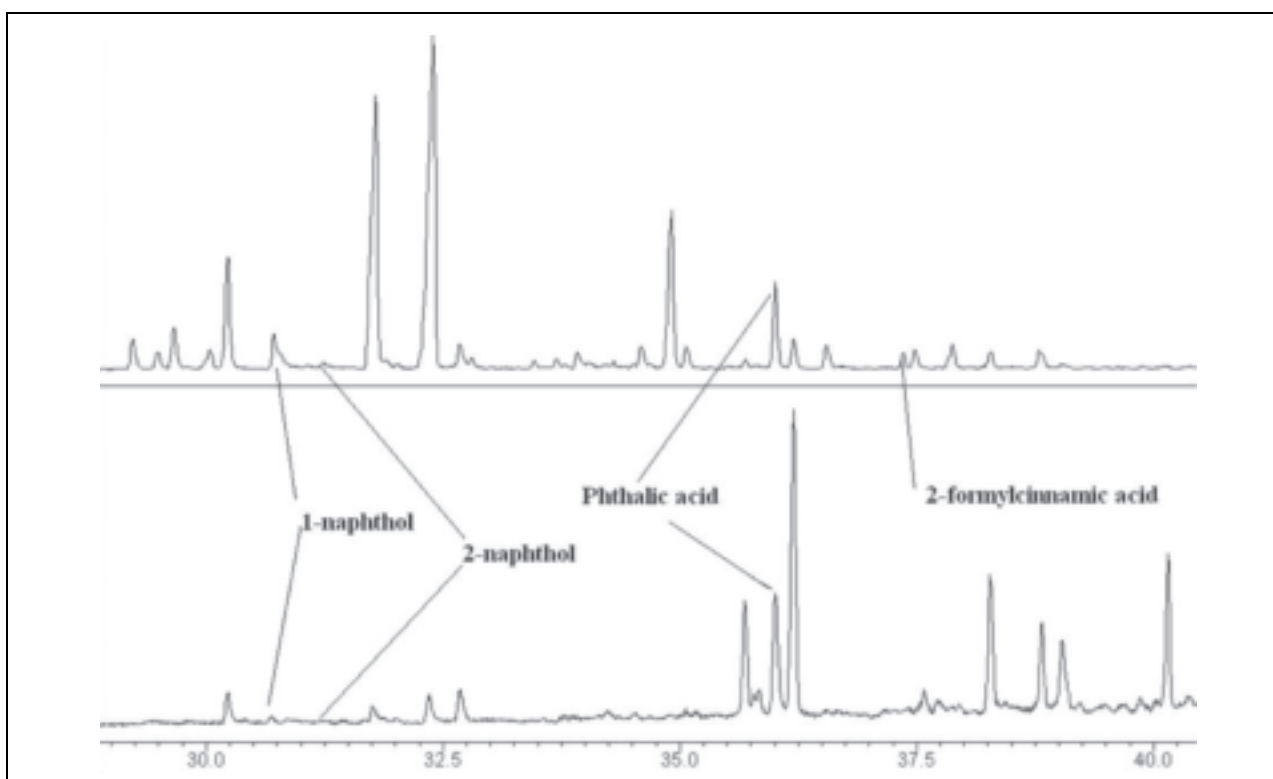


Figure 3.8. Products identified from photooxidation of naphthalene using *N,O*-Bis(trimethylsilyl)trifluoroacetamide (BSTFA) derivatisation.

ring-retaining oxidation products such as naphthol, nitronaphthalene, 2-formyl-cinnamaldehyde and phthalaldehyde. In fact, the peaks at 157 and 173 in the negative ion mass spectrum are tentatively attributed to nitronaphthalene. All of these species have a strong absorption at 266 nm so it is expected that these aromatic compounds will be easily detected using the ATOFMS. The spectra obtained nearly 4 h later were very different. The larger hydrocarbon fragments showed a significantly reduced intensity, suggesting that the ring-retaining products may have reacted further.

In addition, increased signals were observed for CN^- , CNO^- , $\text{C}_2\text{H}_3\text{O}^-$ and COOHCOO^- , indicating that organic nitrates and oxidised organics were formed in the particle phase.

Further insight into the temporal evolution of these species can be gained from Fig. 3.10. While the signal intensity for CN^- (m/z -26), CNO^- (m/z -42) and $\text{C}_2\text{H}_3\text{O}^-$ (m/z -43) all showed a similar increase during irradiation, as soon as the lights were switched off, CN^- and CNO^- did not increase any further, indicating that no new C–N bonds were formed. However, the signal due to $\text{C}_2\text{H}_3\text{O}^-$ continued to increase in the dark, indicating that particle-phase oxidation was maintained, even under dark conditions. This is a particularly interesting result and indicates that the ATOFMS will be useful for investigating particle-phase kinetics and particle-ageing processes.

The results of these preliminary experiments are very encouraging. They confirm that the ATOFMS is capable of monitoring chemical changes in SOA in real time and that naphthalene is an excellent system for exploring the full potential of the technique.

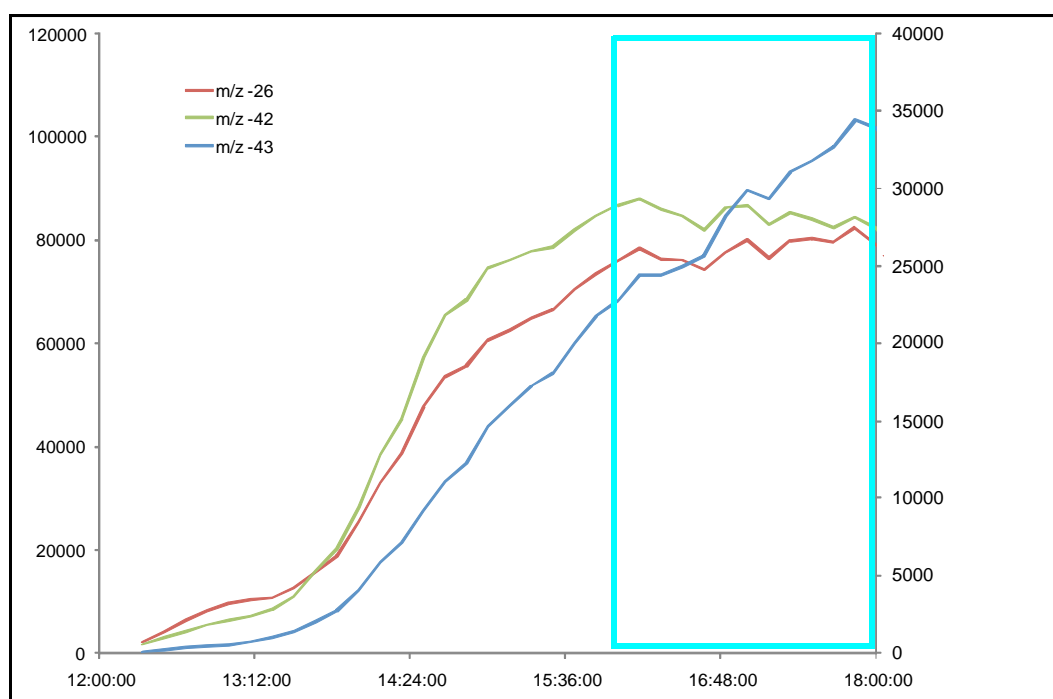


Figure 3.10. Temporal trend for various negative ions during naphthalene secondary organic aerosol photooxidation. The boxed area represents the period when the lights were switched off.

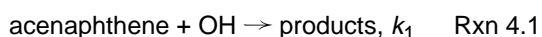
4 Experiments on Photooxidation of Acenaphthene and Acenaphthylene

4.1 Kinetic Studies

4.1.1 Experimental

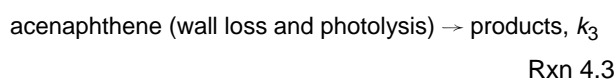
All the experiments were carried out in a 3,910-l cylindrical chamber consisting of an FEP Teflon foil tube (4.1 m long, 1.1 m diameter and 0.127 mm in thickness, supplied by Foiltec, Bremen) closed at both ends by FEP foil-covered aluminium plates.

Rate coefficients for the reactions of OH and NO₃ radicals and O₃ with acenaphthene and acenaphthylene were determined using a relative rate method in which the relative disappearance rates of the acenaphthene and acenaphthylene and the reference compound, whose rate coefficient with the reactive species (OH, NO₃ or O₃) is known, were measured in the presence of either OH, NO₃ or O₃, e.g. for the OH radical reaction with acenaphthene:



where k_1 and k_2 are the rate coefficients for the reactions of the acenaphthene and reference with OH radicals, respectively. Additionally, acenaphthene, acenaphthylene and the reference hydrocarbons could be lost by deposition to the reactor walls or by photolysis.

The combined dark-wall loss and photolysis for acenaphthene and acenaphthylene was found to obey first-order kinetics and can be represented by, e.g. acenaphthene:



where k_3 is the combined dark loss and photolysis rate of the acenaphthene.

However, the losses through wall deposition and photolysis were negligible for the reference compounds used in the experiments.

Equation 4.1 was used to evaluate the kinetic data:

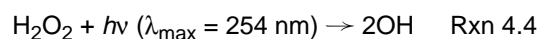
$$\ln \left\{ \frac{[\text{acenaphthene}]_{t_0}}{[\text{acenaphthene}]_t} \right\} - k_3(t - t_0) = \frac{k_1}{k_2} \times \ln \left\{ \frac{[\text{reference}]_{t_0}}{[\text{reference}]_t} \right\} \quad \text{Eqn 4.1}$$

where t_0 is the time at which the reaction is initiated, t is the time at which the IR spectrum was recorded, $[\text{acenaphthene}]_{t_0}$ and $[\text{reference}]_{t_0}$ are the concentrations of the acenaphthene and reference compound, respectively, at time t_0 , $[\text{acenaphthene}]_t$ and $[\text{reference}]_t$ are the corresponding concentrations at time t , k_1 and k_2 are the rate coefficients for the reactions of the acenaphthene and reference with OH radicals, respectively, and k_3 is the combined dark loss and photolysis rate of the acenaphthene. Plots of $\ln([\text{acenaphthene}]_{t_0} / [\text{acenaphthene}]_t) - k_3(t - t_0)$ vs $\ln([\text{reference}]_{t_0} / [\text{reference}]_t)$ should give straight lines with a slope k_1/k_2 . The absolute rate coefficient k_1 can be derived from the rate coefficient ratio k_1/k_2 using the known rate coefficient k_2 .

The rate coefficients for the reactions of the OH radical with acenaphthylene and those of the NO₃ radicals and O₃ with acenaphthene and acenaphthylene were determined in a manner similar to that described above for the OH reactions with acenaphthene.

4.1.1.1 OH radical reaction

The photolysis of H₂O₂ (Rxn 4.4) was used as OH radical precursor:

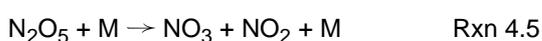


Isoprene was used as the reference compound. The initial concentrations of the reactants, i.e. acenaphthene and acenaphthylene, and isoprene were ~1–2.5 ppm (1 ppm = 2.46 × 10¹³ molecules/cm³ at 298 K) and ~2 ppm, respectively. The dark-wall loss and photolysis rates for the reactants were determined by separate experiments, where only the reactants and

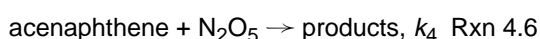
isoprene were introduced into the chamber and the combined wall loss and photolysis rates were measured by switching on the UV lamps in the chamber. As mentioned above, the decay of the reactants was observed to obey first-order kinetics and no decay of isoprene was observed. The reactants were monitored in the IR at the following wavenumbers (in cm^{-1}): acenaphthene at 784.0, acenaphthylene at 773.0 and 832.8, and isoprene at 893.4 and 905.9.

4.1.1.2 NO_3 radical and O_3 reactions

NO_3 radicals were produced by the thermal dissociation of N_2O_5 prepared in solid form:



N_2O_5 was added to the chamber by passing air over the surface of solid N_2O_5 , which was placed in a cold trap at -50°C . The experiments on the reaction of NO_3 with acenaphthene were performed by one addition of N_2O_5 to a mixture of acenaphthene and reference compound; however, those of NO_3 with acenaphthylene were performed by multiple additions of N_2O_5 to the chamber. However, for NO_3 radical reaction with acenaphthene the following reactions have to be taken into account (Atkinson and Aschmann, 1988):



Equation 4.2 was used to evaluate the kinetic data for the NO_3 reaction (Atkinson and Aschmann, 1988):

$$\ln \left\{ \frac{[\text{acenaphthene}]_{t_0}}{[\text{acenaphthene}]_t} \right\} - k_3(t - t_0) = \frac{k_1 + k_4 K[\text{NO}_2]}{k_2} \times \ln \left\{ \frac{[\text{reference}]_{t_0}}{[\text{reference}]_t} \right\} \quad \text{Eqn 4.2}$$

where t_0 is the time at which the reaction is initiated, t is the time at which the IR spectrum was recorded, $[\text{acenaphthene}]_{t_0}$ and $[\text{reference}]_{t_0}$ are the concentrations of the acenaphthene and reference compound, respectively, at time t_0 , $[\text{acenaphthene}]_t$ and $[\text{reference}]_t$ are the corresponding concentrations at time t , k_1 and k_2 are the rate coefficients for the reactions of the acenaphthene and reference with

OH/NO_3 radicals, respectively, k_3 is the dark loss rate of acenaphthene, k_4 is the rate coefficient for the reaction of acenaphthene with N_2O_5 , and K is the equilibrium constant for Rxn 4.4 and $[\text{NO}_2]$ is the NO_2 concentration in a given experiment. Plots of $\ln([\text{acenaphthene}]_{t_0} / [\text{acenaphthene}]_t) - k_3(t - t_0)$ vs $\ln([\text{reference}]_{t_0} / [\text{reference}]_t)$ in Eqns 4.1 and 4.2 should give straight lines with a slope k_1/k_2 in Eqn 4.1 or $(k_1 + k_4 K[\text{NO}_2]) / k_2$ in Eqn 4.2. The absolute rate coefficient k_1 can be derived from the rate coefficient ratios using either the known rate coefficient k_2 in Eqn 4.1 or k_2 , k_4 , K and measured $[\text{NO}_2]$ in Eqn 4.2. The NO_2 concentration was measured by a calibrated IR spectrum of NO_2 .

Similarly for the investigations on the reaction of O_3 with acenaphthene, only one addition of O_3 was made to premixed mixtures containing acenaphthene, CO and reference compound; however, O_3 was added step-wise in the acenaphthylene experiments. One hundred litres of CO were introduced into the chamber prior to addition of O_3 in order to scavenge more than 95% of OH radicals produced in the reaction system. Ozone was generated as a mixture in O_2 by passing O_2 through an O_3 generator.

The initial concentrations of the reactants and references for the NO_3 and O_3 experiments were approximately: acenaphthene and acenaphthylene 2–3 ppm, reference hydrocarbons ~2 ppm. The reactants and references used in the experiments were monitored at the following wavenumbers (in cm^{-1}): acenaphthene at 784.0; acenaphthylene at 773.0 and 832.8; isoprene at 893.4 and 905.9; 2,3-dimethyl-1,3-butadiene at 895; methacrolein at 934, and cyclopentene at 1,048.3.

4.1.2 Results and discussion

4.1.2.1 OH radical reaction

Figure 4.1 shows the kinetic data plots for the OH radical reaction with acenaphthene and acenaphthylene. As can be seen in the first plot, good linear relationships were found for acenaphthene and acenaphthylene. The rate coefficient ratios k_1/k_2 obtained from Fig. 4.1 are 0.9797 and 1.0818 for acenaphthene and acenaphthylene, respectively. Using an absolute rate coefficient for the reaction of the OH radical with isoprene of k_2 ($\text{OH} + \text{isoprene} = 1.01$

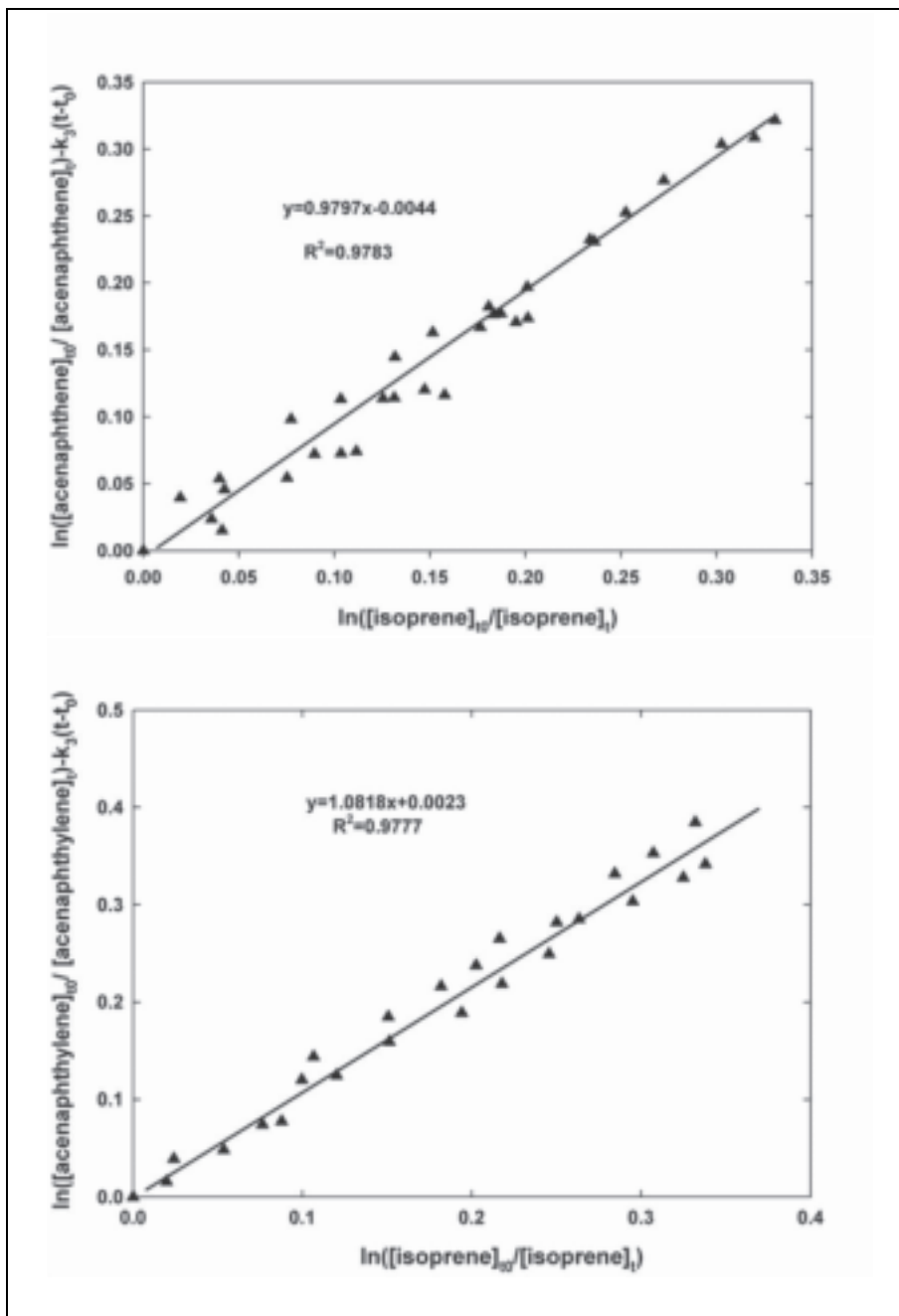


Figure 4.1. Plots of the kinetic data according to [Eqn 4.1](#) for the gas-phase reaction of hydroxyl radicals with acenaphthene (top) and acenaphthylene (bottom).

$\times 10^{-10} \text{ cm}^3/\text{molecule/s}$ as recommended in Calvert et al. (2002), the rate coefficients for OH reaction with acenaphthene and acenaphthylene were derived: k_1 (OH + acenaphthene) = $(9.89 \pm 0.51) \times 10^{-11}$ and k_1 (OH + acenaphthylene) = $(10.9 \pm 0.71) \times 10^{-11} \text{ cm}^3/\text{molecule/s}$.

The corrections to the data for the combined dark decay and photolysis loss of the acenaphthene and

acenaphthylene were approximately 50%. The quoted errors of the rate coefficients k_1 are the least squares standard deviations 2σ .

The rate coefficients for the reactions of the OH radical with acenaphthene and acenaphthylene have previously been reported by several research groups. [Table 4.1](#) summarises the rate coefficients for OH

Table 4.1. Comparison of the rate coefficients (10^{-11} cm³/molecule/s) for the reactions of the hydroxyl radical with acenaphthene and acenaphthylene with values reported in the literature.

Acenaphthene			Acenaphthylene		
$k_1(\times 10^{-11})$ (temp. in K)	Technique	Reference	$k_1(\times 10^{-11})$	Technique	Reference
9.85 ± 0.51 (293 ± 3)	RR	This work	10.9 ± 0.71	RR	This work
5.84 (300)	RR	Klöpffer et al. (1986)	10.9 ± 1.1	RR	Atkinson and Aschmann (1988)
10.2 ± 1.2 (293 ± 3)	RR	Atkinson and Aschmann (1988)	12.76	RR	Banceu et al. (2001)
5.98 ± 0.24 (325)	RR	Brubaker and Hites (1998)	12.4 ± 0.7	RR	Reisen and Arey (2002)
5.68 ± 0.62 (325)	RR	Brubaker and Hites (1998)			
6.67 (295)	RR	Banceu et al. (2001)			
8.0 ± 0.4 (296 ± 2)	RR	Reisen and Arey (2002)			

RR, relative rate technique.

reactions obtained in the peer-reviewed literature and those obtained in the present work.

It is clear from [Table 4.1](#) that the rate coefficients for the reaction of the OH radical with acenaphthene and acenaphthylene obtained in the present work are in good agreement with those measured by Atkinson and Aschmann (1988). The values for acenaphthene obtained by Atkinson and Aschmann and in the present work are higher than those determined by Klöpffer et al. (1986) and Brubaker and Hites (1998) by a factor of ~1.6. It has to be noted that Klöpffer et al. (1986) and Brubaker and Hites (1998) measured the rate coefficient for the OH radical with acenaphthene relative to ethene, cyclohexane and toluene. The reference compounds they used are 7–13 times less reactive than acenaphthene and, as a result, the fractions of the reference and acenaphthene that reacted were significantly disparate, probably causing large uncertainties in their measurements.

On the other hand, Brubaker and Hites (1998) performed their studies at elevated temperatures (~30 degrees higher than other studies); however, they concluded that the rate coefficient for the OH radical reaction with acenaphthene was temperature independent.

Relative to naphthalene, Banceu et al. (2001) obtained the rate coefficient ratios, k_1/k_2 , of 2.9 and 5.8 for the OH radical reactions with acenaphthene and

acenaphthylene, respectively. Using an absolute rate coefficient of 2.3×10^{-10} cm³/molecule/s (Calvert et al., 2002) for the reaction of the OH radical with naphthalene, the rate coefficients for OH reactions with acenaphthene and acenaphthylene were derived and are listed in [Table 4.1](#).

Recently, using a relative kinetic method, Reisen and Arey (2002) reported kinetic studies on OH radical and O₃ reactions with acenaphthene and acenaphthylene. Rate coefficients were obtained of $(8.0 \pm 0.4) \times 10^{-11}$ and $(12.4 \pm 0.7) \times 10^{-11}$ cm³/molecule/s for the reaction of the OH radical with acenaphthene and acenaphthylene, respectively ([Table 4.1](#)). The rate coefficient for acenaphthene is lower than in Atkinson and Aschmann (1988) and the present work, but the value for acenaphthylene was in good agreement with that obtained by Banceu et al. (2001), which is higher than other determinations. It should be noted that the initial concentrations of the reference compounds employed in the studies of Reisen and Arey (2002) were higher than acenaphthene and acenaphthylene by factors of 13–26, which might result in uncertainties in monitoring the decay of the reference compound. Moreover, Reisen and Arey (2002) monitored the reactants and the reference compound in different ways. They analysed the reference compound by collecting gas samples by gas-tight syringe from the chamber and injecting directly into the GC-FID. Acenaphthene and acenaphthylene were monitored by

collecting the gas sample from the chamber onto a solid absorbent cartridge, with subsequent GC-FID analysis. However, in the present work both the reactants and reference hydrocarbons were analysed by in situ long-path FTIR, which avoided the potential artefact in the sampling procedures.

It is expected that the initial reaction of OH + acenaphthene is slower than that for OH + acenaphthylene because the latter has a conjugated Π bond which facilitates the OH radical attack. However, from the present work and the studies of Atkinson and Aschmann (1988), the reactivity of acenaphthene and acenaphthylene towards OH radicals is quite similar. Because of the lack of the

determinations on the rate coefficients for the OH radical reactions and the complexity of the PAHs, it is currently not possible to compare the experimental results with any theoretical calculations. Until more information from kinetic studies on acenaphthene and acenaphthylene becomes available no further speculation is warranted.

NO₃ radical reaction

Figure 4.2 shows the kinetic data plots for the NO₃ radical reaction with acenaphthene and acenaphthylene. The rate coefficient ratios k_1/k_2 shown in Fig. 4.2 are 0.8558 (relative to isoprene) for acenaphthene and 2.1041 (relative to 2,3-dimethyl-1,3-butadiene) for acenaphthylene. Using these ratios

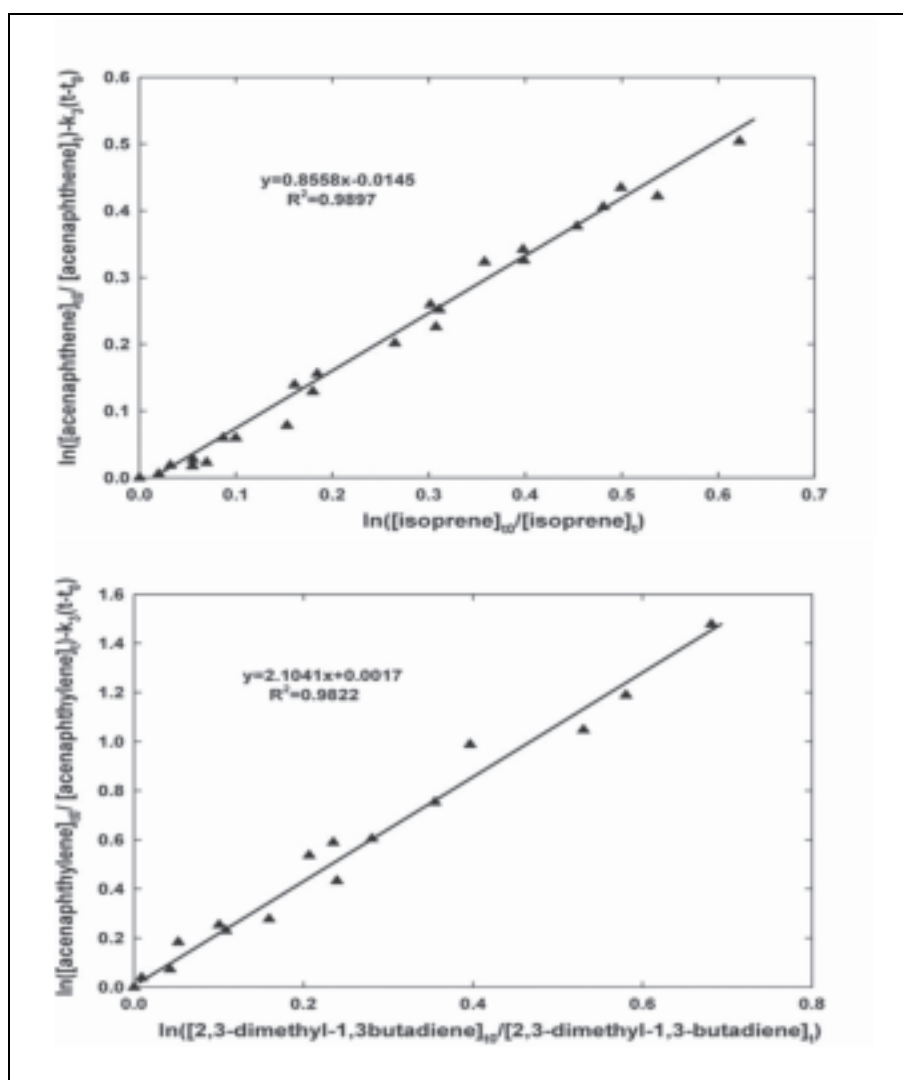


Figure 4.2. Plots of the kinetic data according to Eqn 4.1 for the gas phase reaction of nitrate radicals with acenaphthene (top) and acenaphthylene (bottom).

in combination with $k_2 = 6.78 \times 10^{-13} \text{ cm}^3/\text{molecule/s}$ for isoprene and $k_2 = 2.1 \times 10^{-12} \text{ cm}^3/\text{molecule/s}$ for 2,3-dimethyl-1,3-butadiene (Atkinson and Arey, 2003) leads to the rate coefficients k_1 for the reaction of NO_3 with acenaphthene and acenaphthylene as $k_1 = (5.83 \pm 0.27) \times 10^{-13}$ and $k_1 = (4.42 \pm 0.32) \times 10^{-12} \text{ cm}^3/\text{molecule/s}$, respectively.

Atkinson and Aschmann (1988) reported rate coefficients of $(4.59 \pm 2.46) \times 10^{-13}$ and $(5.45 \pm 0.47) \times 10^{-12} \text{ cm}^3/\text{molecule/s}$ for the reactions of the NO_3 radical with acenaphthene and

acenaphthylene, respectively. These are the only determinations on the rate coefficients for NO_3 radical reaction with acenaphthene and acenaphthylene available in the peer-reviewed literature. The rate coefficients obtained in the present work are slightly different from those reported by Atkinson and Aschmann (1988); however, they agree quite well when the errors are taken into account.

O₃ radical reaction

Figure 4.3 shows examples of the kinetic data plotted according to Eqn 4.1 for the reactions of O_3 with

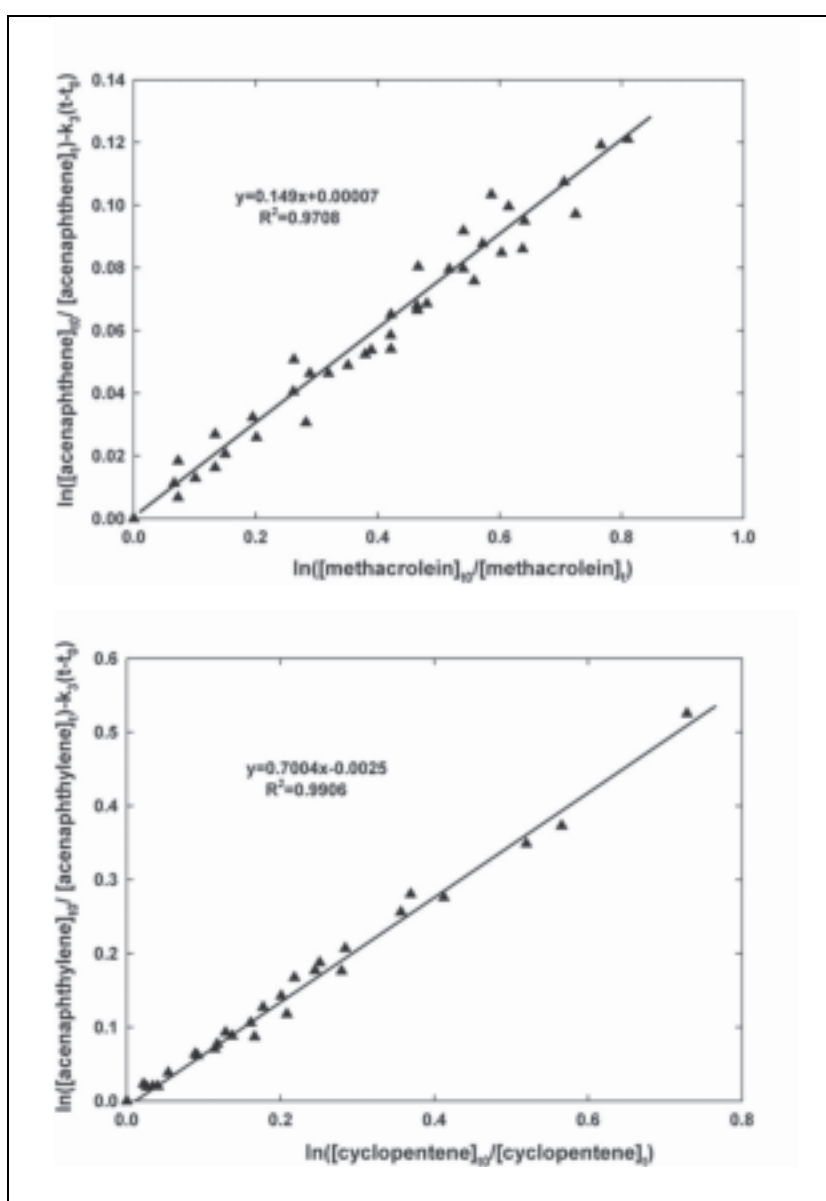


Figure 4.3. Plots of the kinetic data according to Eqn 4.1 for the gas phase reaction of ozone with acenaphthene (top) and acenaphthylene (bottom).

acenaphthene and acenaphthylene. The reference hydrocarbons employed were methacrolein and cyclopentene for acenaphthene and acenaphthylene, respectively, and the rate coefficient ratios k_1/k_2 obtained from plots of the data were 0.149 and 0.7004 for acenaphthene and acenaphthylene, respectively. Using these ratios in combination with k_2 ($\text{O}_3 + \text{methacrolein}$) = 1.2×10^{-18} $\text{cm}^3/\text{molecule/s}$ and k_2 ($\text{O}_3 + \text{cyclopentene}$) = 5.7×10^{-16} $\text{cm}^3/\text{molecule/s}$ (Atkinson and Arey, 2003) leads to the rate coefficients for the reaction of O_3 with acenaphthene and acenaphthylene as $(1.8 \pm 0.1) \times 10^{-19}$ and $(3.99 \pm 0.15) \times 10^{-16}$ $\text{cm}^3/\text{molecule/s}$, respectively.

Only an upper limit of 5×10^{-19} $\text{cm}^3/\text{molecule/s}$ for the rate coefficient of ozonolysis of acenaphthene was reported by Atkinson and Aschmann (1988). The rate coefficient for the O_3 reaction with acenaphthene obtained in the present work was lower than this limit. Atkinson and Aschmann also measured the rate coefficient for the ozonolysis of acenaphthylene as 5.5×10^{-16} $\text{cm}^3/\text{molecule/s}$, which is more than three times higher than that reported by Reisen and Arey (2002) and 1.4 times higher than the present work. The reason for such big discrepancies between the different research groups is currently not known. Further determinations are, therefore, necessary in order to evaluate the reaction rate of acenaphthylene with O_3 .

Atmospheric lifetimes

The results from these kinetics experiments can be used to calculate the atmospheric lifetimes of these PAHs. The atmospheric lifetime is defined as $1/k[\text{species}]$, where k is the rate coefficient for the

reaction of the reactive species (OH , NO_3 or O_3) with PAHs and $[\text{species}]$ is the concentration of the reactive species, respectively. Using the rate coefficients obtained in the present work and the average tropospheric concentrations of the OH and NO_3 radicals and an O_3 value of $\sim 1 \times 10^6$ (24-h yearly global average (Prinn et al., 1995)), 5.4×10^8 (24-h average concentration in rural air mass (Platt and Heintz, 1994)) and 7×10^{11} (24-h average concentration (Logan, 1985)) molecules/cm^3 , respectively, the atmospheric lifetimes of acenaphthene and acenaphthylene with respect to the degradation reaction with the OH and NO_3 radicals and O_3 were estimated and are listed in Table 4.2. From Table 4.2, it is clear that the OH and NO_3 radicals contribute to the main degradation of both PAHs in daytime and night-time, respectively. From the rate constant measurements, it is known that, compared with acenaphthene, acenaphthylene reacts much faster with O_3 . The O_3 reaction seems not to contribute to the atmospheric degradation of acenaphthene but does contribute to the degradation of acenaphthylene. The short lifetimes of acenaphthene and acenaphthylene with respect to the reactions of the OH and NO_3 radicals and the acenaphthylene reaction with O_3 show that both PAHs will be quickly degraded when emitted to the atmosphere and will only be actively involved in tropospheric chemistry on local to regional scales. From the test experiment of this work and a previous study of Atkinson and Aschmann (1988), the loss of acenaphthene and acenaphthylene due to photolysis under atmospheric conditions is of minor importance.

Table 4.2. Atmospheric lifetimes of acenaphthene and acenaphthylene with respect to the degradation reaction with hydroxyl (OH) and nitrate (NO_3) radicals and ozone (O_3).

	T_{OH}^{a}	$T_{\text{NO}_3}^{\text{b}}$	$T_{\text{O}_3}^{\text{c}}$
Acenaphthene	2.8 (h)	0.9 (h)	92 (days)
Acenaphthylene	2.5 (h)	0.1 (h)	1.0 (h)

^aThe average tropospheric concentration of the OH radical was ca 1×10^6 molecules/cm^3 (24-h yearly global average (Prinn et al., 1995)).

^bThe average tropospheric concentration of the NO_3 radical was 5.4×10^8 molecules/cm^3 (24-h average concentration in rural air mass (Platt and Heintz, 1994)).

^cThe average tropospheric concentration of O_3 was 7×10^{11} molecules/cm^3 (24-h average concentration (Logan, 1985)).

4.2 Product Studies

4.2.1 Experimental

The product study on the OH-radical-initiated oxidation of acenaphthene was performed at 298 ± 5 K in purified air at atmospheric pressure in a 6,500-l rectangular FEP Teflon chamber.

Nitrous acid was synthesised by adding a 1% NaNO_2 aqueous solution dropwise into a flask containing 30% sulfuric acid. The initial concentration of acenaphthene was 1–2 ppm. Its decay was determined by an online GC-FID.

Secondary organic aerosol formation was observed in the OH radical reaction with acenaphthene. The particle size distribution was monitored by an SMPS (TSI Model 3034). A denuder-filter sampling technique was employed to collect the gas- and particulate-phase products. The denuder was again coated with absorbent XAD-4 resin. After collecting the products for 30 min at ~ 10 l/min gas flow, the denuder was extracted twice with 10 ml methanol and followed by sonication for 15 min, while the filter was extracted by sonication for 15 min in 10 ml methanol.

4.2.1.1 Direct GC-MS analysis

Two millilitres of the extracts from the denuder and filter were filtered using a 0.45- μm pore size polytetrafluoroethylene (PTFE) membrane syringe filter and dried under a gentle stream of nitrogen. The residue was dissolved in 200 μl methanol and analysed by GC-MS in both CI and EI modes.

A Varian Saturn 2000 ion-trap GC-MS, which consisted of a Varian CP 3800 GC and a fused silica capillary column (5% diphenyl, 95% dimethylpolysiloxane, 0.25 μm film thickness, 0.25 mm internal diameter, and 30 m in length), was used to analyse the products. The ion source was operated in both CI and EI modes. The oven temperature was started at 40°C, held for 1 min, then ramped to 280°C at 8°C/min, held for 5 min and ramped from 280°C to 310°C at 10°C/min, and held for 1 min. Helium was used as carrier gas at 1 ml/min and methane was used as CI gas. The MS was operated in full scan mode over a mass range of m/z 60–650.

4.2.1.2 PFBHA derivatisation of glyoxal

Glyoxal is expected to be co-produced with a C_{10} ring-opening product, which was not reported in the previous study on the atmospheric oxidation of acenaphthene (Reisen and Arey, 2002) due to a limitation in the analytical method used. Determination of glyoxal derivatised with derivatising agent PFBHA was reported in a previous study of this laboratory (Healy et al., 2008). The same derivatisation method was employed in the present work to detect glyoxal.

The same sampling and extracting procedures described above for denuder and filter samples were applied. Five milligrams of PFBHA were added to the denuder and filter extractions and they were then left in the dark for 2 days. Two millilitres of the solution were filtered using a 0.45- μm pore size PTFE membrane syringe filter, dried under a gentle stream of nitrogen, followed by dissolving in 100 μl *n*-hexane and then analysed with GC-MS in EI mode. The oven temperature programme adapted from a previous study from this laboratory (Healy et al., 2008) was as follows: 60°C held for 1 min, then ramped from 60°C to 100°C at 5°C/min, from 100°C to 280°C at 10°C/min and from 280°C to 310°C at 30°C/min, and then held for 5 min. Helium was used as the carrier gas at 1 ml/min. The MS was operated in EI and in full scan modes over a mass range of m/z 60–650.

4.2.2 OH radical reaction with acenaphthene

The gas- and particulate-phase products from acenaphthene reaction with the OH radical were analysed using two different methods, i.e. direct injection of methanol extracts of the denuder and filter samples and derivatisation of the extracts with PFBHA to detect glyoxal. The GC-MS total ion chromatograms, (A) and (B) in [Fig. 4.4](#), show the products identified from the direct injection of the chamber samples from the denuder and filter, respectively.

The identified products and suggested chemical structure are listed in [Table 4.3](#). As mentioned above the only product study on the reaction of acenaphthene with the OH radical was reported by Reisen and Arey (2002). Using atmospheric pressure ionisation (API)-MS, Reisen and Arey reported the aromatic ring-opened product of $[\text{M}+\text{H}]^+ = 161$ (with a molecular

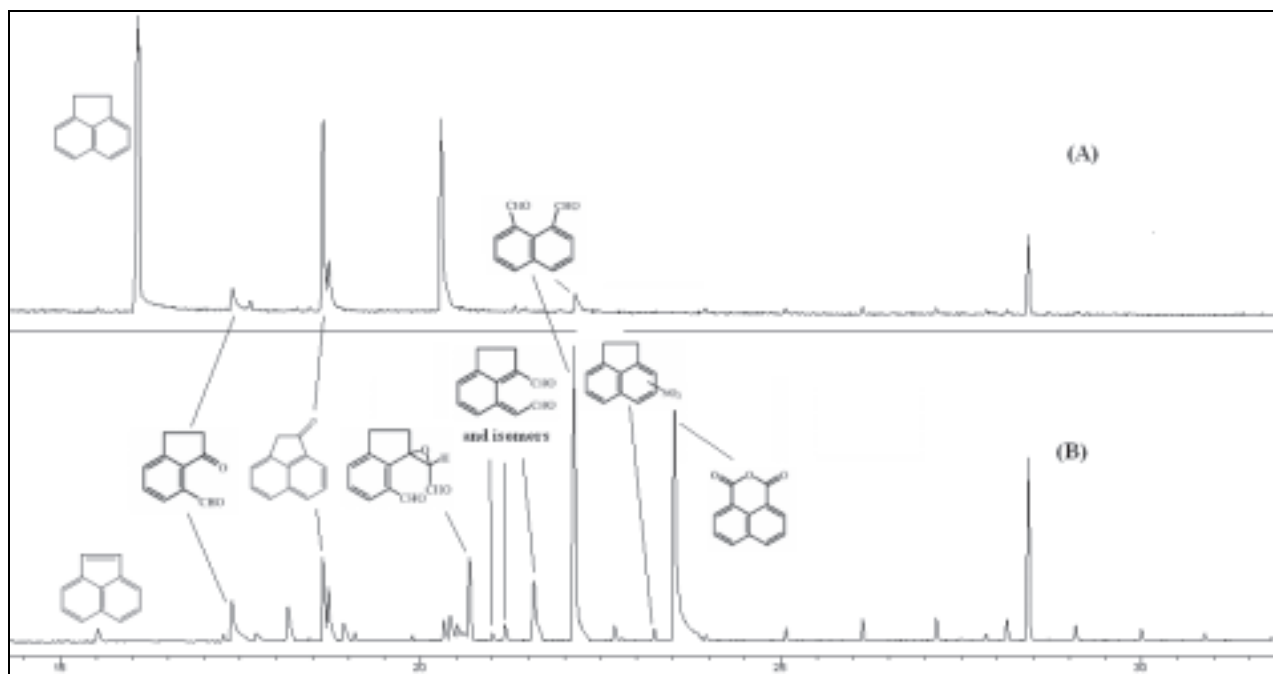


Figure 4.4. Gas chromatography–mass spectrometry total ion chromatograms of denuder (A) and filter (B) samples from the acenaphthene reaction with hydroxyl radicals.

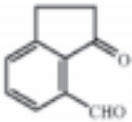
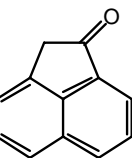
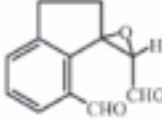
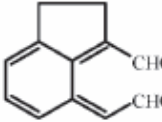
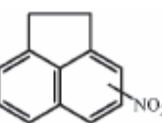
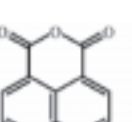
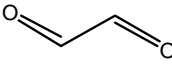
formula of $C_{10}H_8O_2$) and $[M+H]^+ = 187$ (dialdehyde with a molecular formula of $C_{12}H_{10}O_2$) and an epoxide of $[M+H]^+ = 203$ (with a molecular formula of $C_{12}H_{10}O_3$), with that of $[M+H]^+ = 161$ being the major one. However, different from the observations made by Reisen and Arey (2002), the gas-phase products collected on the denuder coupled with GC-MS-CI analysis in the present work are those of $[M+H]^+ = 161$, $[M+H]^+ = 169$ and $[M+H]^+ = 185$ with the product of $[M+H]^+ = 169$ being the most intense peak in the chromatogram (Fig. 4.4A).

As in Reisen and Arey's study, the product of $[M+H]^+ = 161$ can be attributed to the C_{10} ring-opening product. The two peaks of $[M+H]^+ = 169$ and $[M+H]^+ = 185$ were not reported by Reisen and Arey (2002) in the reaction of acenaphthene and OH radicals. The GC-MS-EI analysis of the same products shows that the product of $M = 168$ gives a fragmentation of 140, indicating the presence of a carbonyl group ($-C(O)$) in the molecule, while the product of $M = 184$ shows fragmentations of 155 (loss of a $-CHO$ group from the molecule) and 127 (loss of a carbonyl group from the fragmentation of 155), suggesting the presence of both an aldehyde group

and a $-C(O)$ group, either from carbonyl or aldehyde. Based on the reaction mechanism discussed below, the products of $[M+H]^+ = 169$ from CI mode (or $[M]^+ = 168$ from EI mode) and $[M+H]^+ = 185$ from CI mode (or $[M]^+ = 184$ from EI mode) are tentatively attributed to acenaphthene-1-one (MW = 168) and naphthalene-1,8-dicarbaldehyde (MW = 184) (Fig. 4.4A and Table 4.2), respectively.

The product of $[M+H]^+ = 161$ was again identified as a major product in the fibre sample of Reisen and Arey (2002). However, from Fig. 4.4B and Table 4.2, it is clear that the main products in the denuder sample of this work are identified as acenaphthene-1-one, naphthalene-1,8-dicarbaldehyde and 1,8-naphthalene anhydride. 1,2-Acenaphthylenedione, observed in the Reisen and Arey study (2002) and attributed by the authors to the sampling artefact formed from naphthalene-1,8-dicarbaldehyde during the desorption process, was not observed in the present work. The formation of naphthalene-1,8-dicarbaldehyde can result from the OH radical addition to the acenaphthylene impurity which can be seen in the denuder sample (Fig. 4.4B) (Reisen and Arey, 2002). However, the significant ion peak of naphthalene-1,8-

Table 4.3. Products identified in the gas and particulate phases from the reaction of acenaphthene with the hydroxyl radical.

Compound		Retention time (min)	Molecular mass	m/z (CI mode)	Gas phase	Particle phase
$C_{10}H_8O_2$		17.39	160	161 (M+1)	Yes	Yes
Acenaphthene-1-one		18.67	168	169 (M+1)	Yes	Yes
$C_{12}H_{10}O_3$		20.68	202	203 (M+1)	No	Yes
Dialdehyde ¹		21.01 21.17 21.58	186	187 (M+1)	No	Yes
Naphthalene-1,8-dicarbaldehyde		22.13	184	185 (M+1)	Yes	Yes
Nitroacenaphthene		23.25	199	200 (M+1)	No	Yes
1,8-Naphthalic anhydride		23.52	198	199 (M+1)	No	Yes
Glyoxal		20.32 ² 20.41 ²	448	181 ³ 448 ³	Yes	Yes

¹Three peaks on the chromatogram having similar mass spectra are believed to be the isomers of dialdehydes (Reisen and Arey, 2002).

²It should be noted that glyoxal-*O*-(2,3,4,5,6-pentafluorobenzyl)-hydroxylamine is analysed at different gas chromatogram-mass spectrometry conditions with other photooxidation products.

³Mass spectrum for glyoxal-*O*-(2,3,4,5,6-pentafluorobenzyl)-hydroxylamine is obtained under electron ionisation mode.

dicarbaldehyde in the particulate phase in [Fig. 4.4B](#) suggests that, rather than being formed from acenaphthylene impurity, it should be formed from the reaction of acenaphthene. As discussed below the formation of naphthalene-1,8-dicarbaldehyde could result from H-atom abstraction from the cyclopenta-fused ring of acenaphthene. The identification of another major peak in both the gas and particulate phases of the present work, acenaphthene-1-one, which was not reported by Reisen and Arey (2002), could be attributed to a sequence product of naphthalene-1,8-dicarbaldehyde and again suggests that H-atom abstraction from the cyclopenta-fused ring of acenaphthene is a definite reaction pathway.

In addition, the peaks of $[M+H]^+ = 203$ and $[M+H]^+ = 200$, observed in the particulate phase of the present work, are attributed to an epoxide with molecular formula $C_{12}C_{10}O_3$ and nitroacenaphthene ([Fig. 4.4](#)) according to the Reisen and Arey (2002) study. There are three products in the particulate phase with the same molecular weight ($[M+H]^+ = 187$) ([Fig. 4.4B](#) and [Table 4.2](#)) and similar mass spectra.

According to Reisen and Arey (2002), they are attributed to dialdehyde isomers (with a molecular formula of $C_{12}H_{10}O_2$) formed via OH radical addition to the aromatic ring of acenaphthene.

As discussed above, since the C_{10} ring-opening product of $[M+H]^+ = 161$ was observed in both the Reisen and Arey (2002) study and the present work, glyoxal should be co-produced in the reaction according to the mechanism proposed by Reisen and Arey (2002). However, the formation of glyoxal was not reported by Reisen and Arey (2002), most probably due to the limitation of the analytical methods employed. The identification of glyoxal was reported in this laboratory from the photooxidation of 1,3,5-trimethylbenzene using the PFBHA derivatisation method (Healy et al., 2008). The same method was applied in the present work to identify glyoxal formed in the photooxidation of acenaphthene.

The GC-MS total ion chromatograms of glyoxal-PFBHA from denuder and filter samples are shown in [Fig. 4.5A](#) and [4.5B](#), respectively, and the GC-MS

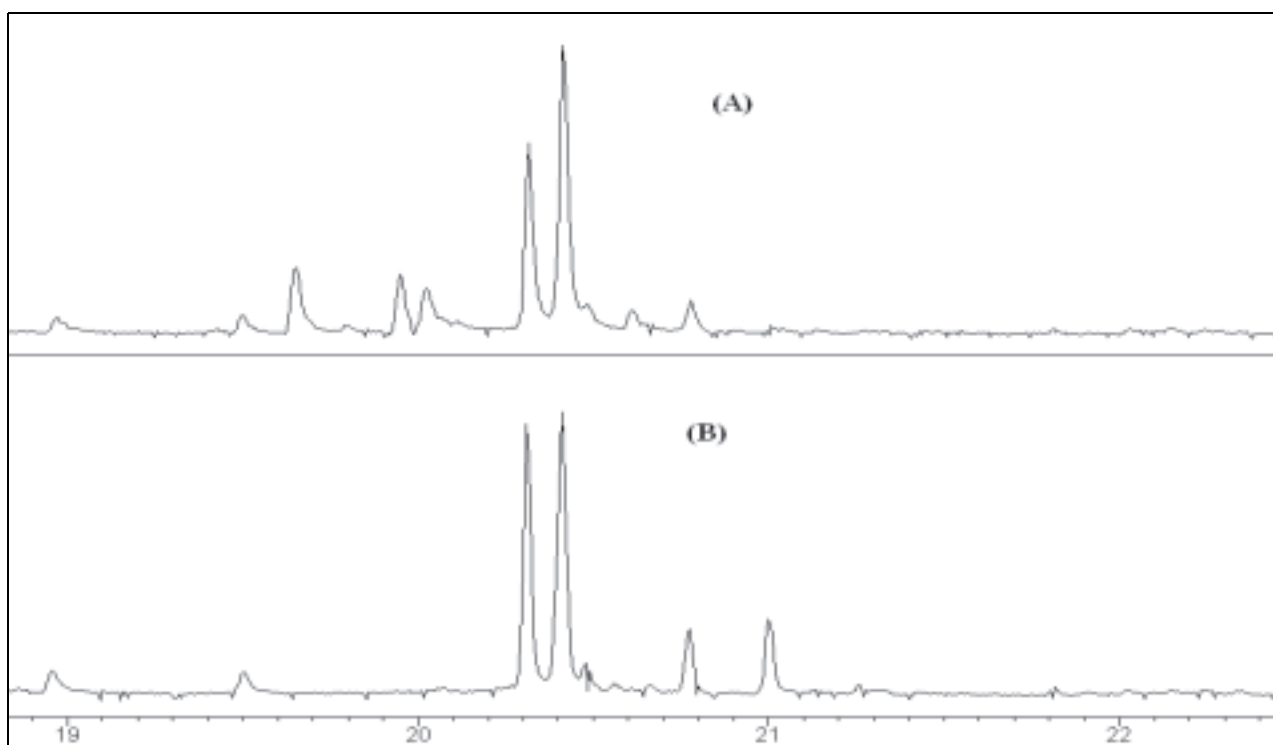


Figure 4.5. Identification of glyoxal in denuder (A) and filter (B) samples with *O*-(2,3,4,5,6-pentafluorobenzyl)-hydroxylamine derivatisation coupled with gas chromatography–mass spectrometry–electron ionisation analysis.

information on glyoxal–PFBHA is listed in [Table 4.2](#). The two glyoxal–PFBHA peaks shown in [Fig. 4.5A](#) and [4.5B](#) are the isomers of the oxime products.

The reaction of acenaphthene with the OH radical is expected to proceed via either the addition of the OH radical to the six-membered aromatic ring or H-atom abstraction from the cyclopenta-fused ring of acenaphthene. The addition of OH to the aromatic ring will form an energy-rich hydroxycyclohexadienyl-type radical, whose further reactions produce dicarbonyls, e.g. those of $[M+H]^+ = 161$, glyoxal, $[M+H]^+ = 187$ and epoxide with $[M+H]^+ = 203$. This reaction pathway has already been outlined by Reisen and Arey (2002).

As shown in [Fig. 4.6](#), H-atom abstraction from the cyclopenta-fused ring of acenaphthene (I) results in the formation of a radical (II). The addition of O_2 to the radical (II) produces a peroxy radical (III). In the presence of NO, the peroxy radical (III) reacts with NO to generate an alkoxy radical (IV), which reacts with O_2 or decomposes to give another radical (VI). The reaction of the alkoxy radical (IV) with O_2 results in the formation of acenaphthene-1-one (V), a major product identified in the present work, while the decomposition of the peroxy radical (IV) gives another radical (VI), which further reacts with O_2 and NO and finally produces naphthalene-1,8-dicarbaldehyde (VIII), another main product observed in the particulate phase of the present work. Since no distinct peak

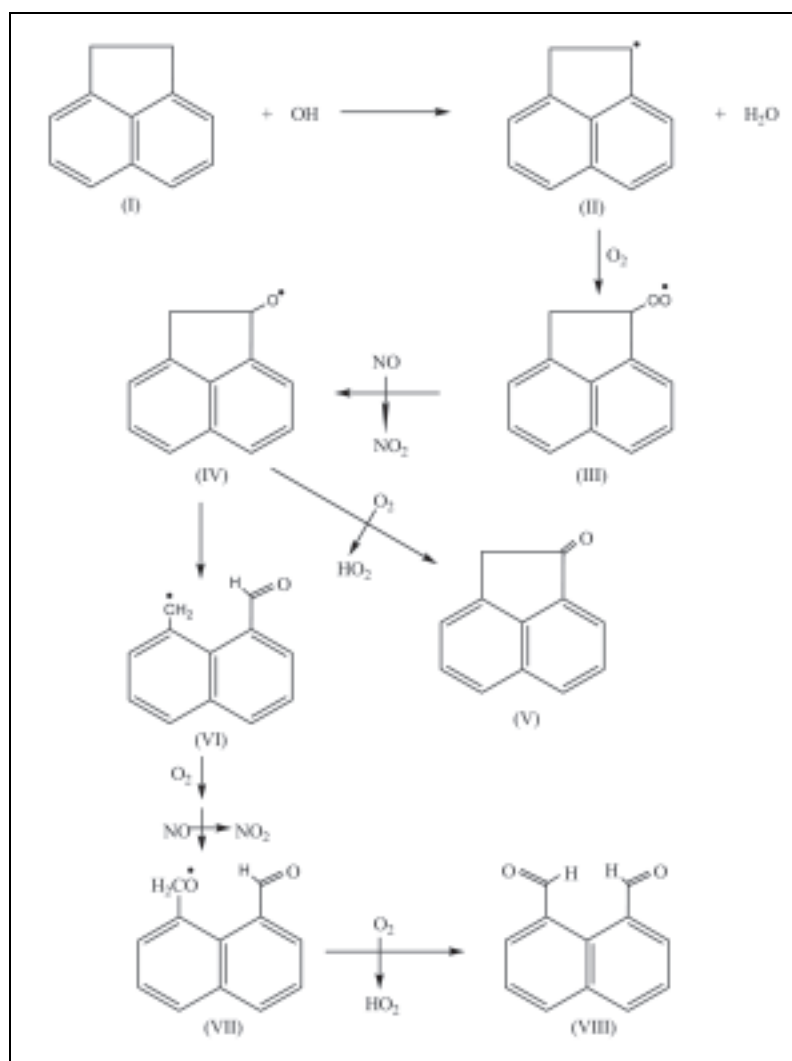


Figure 4.6. Hydrogen-atom abstraction mechanism for the reaction of acenaphthene with the hydroxyl radical.

attributed to either acenaphthene-1-one or naphthalene-1,8-dicarbaldehyde was observed in the Reisen and Arey (2002) study, the author concluded that the H-atom abstraction was a very minor reaction pathway. As discussed above, even the formation of naphthalene-1,8-dicarbaldehyde can be partly attributed to acenaphthylene impurity. The significant peaks of acenaphthene-1-one in the gas-phase sample of the present work clearly indicate that H-atom abstraction from the cyclopenta-fused ring is a major reaction pathway. The reason for such a discrepancy between these two reaction systems is currently not known. However, the very similar OH radical rate coefficients for the reaction of acenaphthene and acenaphthylene with the OH radical indicate that the H-atom abstraction from acenaphthene contributes to such a high reactivity towards the OH radical.

4.2.3 OH radical reaction with acenaphthylene

Gas- and particulate-phase products were collected using the denuder-filter sample system and analysed by GC-MS. [Figure 4.7](#) shows the GC-MS total ion chromatograms for the products from the direct

injection of the sample extracts from the denuder (A) and filter (B). Based on the previous study of Reisen and Arey (2002) and the present work on the reaction of acenaphthene with OH radicals, the chemical structures of the products are listed in [Table 4.4](#). It should be noted that the product with a retention time of 18.68 min and a molecular weight of 168 ([Table 4.4](#)) was attributed to an epoxide by Reisen and Arey (2002). However, based on the results obtained in this work for acenaphthene, this product is attributed to acenaphthene-1-one due to the fact that both have the same retention time and mass spectra (as discussed above).

Two products with a molecular mass of 184 were detected. This finding is in contrast to the study of Reisen and Arey, where only one product with a molecular weight of 184 was detected. Based on the results obtained for acenaphthene, the compound with a retention time of 22.22 min is attributed to naphthalene-1,8-dicarbaldehyde, while the product with a retention time of 21.76 min and a similar mass spectrum to naphthalene-1,8-dicarbaldehyde is

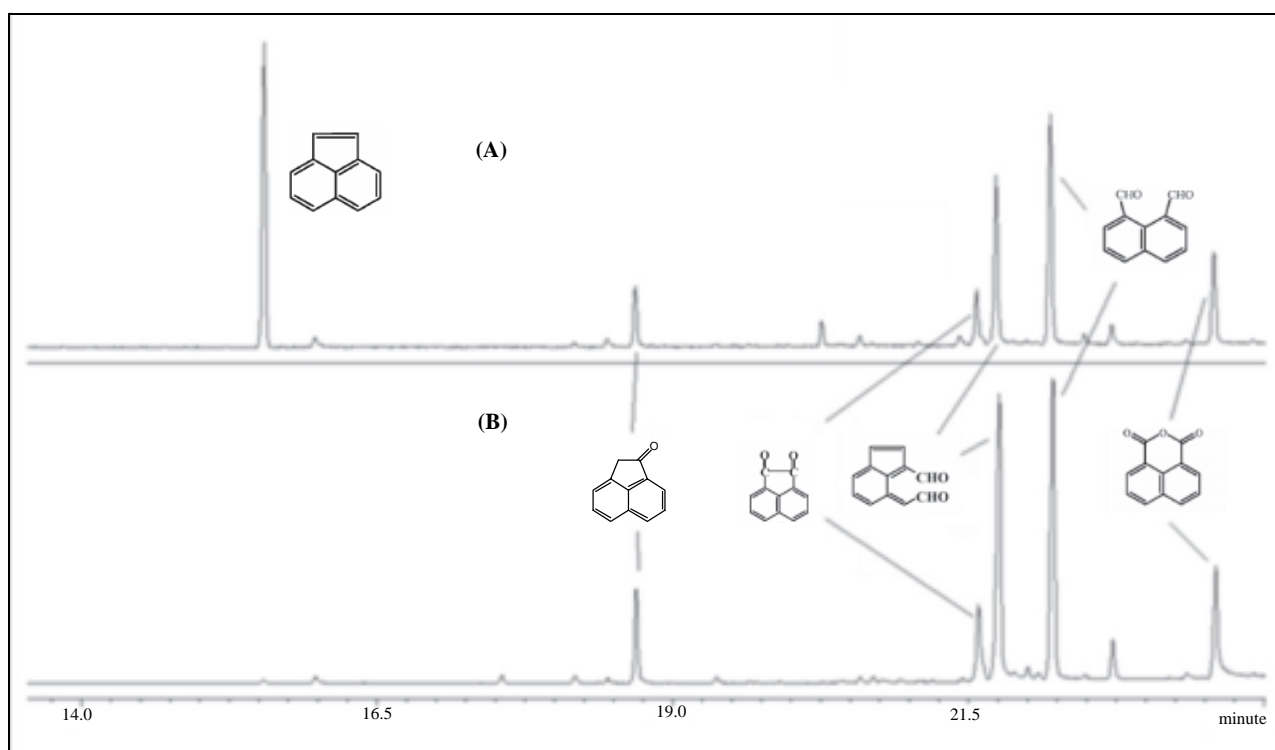
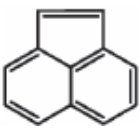
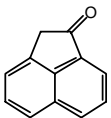
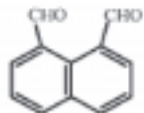


Figure 4.7. Gas chromatography–mass spectrometry total ion chromatograms of denuder (A) and filter (B) samples from the acenaphthylene reaction with hydroxyl radicals.

Table 4.4. Products identified in the gas and particulate phases from the reaction of acenaphthylene with the hydroxyl radical.

Compound		Retention time (min)	Molecular mass	m/z (CI mode)	Gas phase	Particle phase
Acenaphthylene		15.55	152	153 (M+1)	Yes	No
Acenaphthene-1-one		18.68	168	169 (M+1)	Yes	Yes
Acenaphthoquinone		21.59	182	183 (M+1)	Yes	Yes
Dialdehyde		21.76	184	185 (M+1)	Yes	Yes
Naphthalene-1,8-dicarbaldehyde		22.22	184	185 (M+1)	Yes	Yes
1,8-Naphthalic anhydride		23.52	198	199 (M+1)	Yes	Yes

attributed to an aromatic dialdehyde (Table 4.4). Acenaphthoquinone, which was not observed in the acenaphthene-OH reaction system, was identified as one of the major products in the acenaphthylene reaction.

From Fig. 4.7 and Table 4.4, it is clear that both aromatic ring-retaining and ring-opening products are observed as major products, indicating that the addition of OH to the aromatic ring and the unsaturated cyclopenta-fused ring are both important reaction pathways.

5 Toxicological Tests

5.1 Experimental

Reactive oxygen species produced from extracts of the SOA collected during the simulation chamber experiments were determined using a method recently developed in the laboratory of Prof. J.J. Heffron, Biochemistry Department, University College Cork. The method, which is a convenient and effective alternative to in-vitro and in-vivo tests, relies on the ability of particulate components, such as quinones, to catalyse the reduction of oxygen to anion superoxide (O_2^-). The chemical assay involves the reaction of oxygenated organic compounds with dithiothreitol (DTT) to produce the ROS and is based on the work of Li et al. (2003) and Cho et al. (2004).

The DTT assay was applied to filter samples of SOA collected from the photooxidation of three PAHs (naphthalene, acenaphthene and acenaphthylene). After sampling, the filters were extracted with dichloromethane, dried under nitrogen and then dissolved in dimethyl sulfoxide (DMSO). The consumption of DTT was determined after 10 min of incubation (37°C) of the SOA extracts with DTT (0.25 M Tris-HCl, pH 8.9) by adding 5,5'-dithio-bis-2-

nitrobenzoic acid (DTNB) to the solution to form a stable compound which was detected by colorimetry at 414 nm.

5.2 Results and Discussion

A typical DTT calibration curve was obtained by plotting the resulting absorbance from the DTT-DTNB reaction against the DTT concentration (Fig. 5.1). Using this curve, the amount of DTT consumed by the SOA extracts was determined and the results are plotted in Fig. 5.2. Different sample concentrations were chosen for the three SOA extracts in order to consume 2–20% of the DTT. As shown in Fig. 5.2, there is a linear relationship between the sample concentration and the amount of DTT consumed. The slopes of the straight lines are 3.64, 1.63 and 7.20 for naphthalene, acenaphthene and acenaphthylene, respectively. This indicates that the SOA generated from acenaphthylene consumed the highest amount of DTT, while SOA from acenaphthene consumed the lowest amount. Since the quinone formation yields from these three PAHs were not measured, the relationship between quinone concentrations and DTT consumption could not be quantified. Nevertheless,

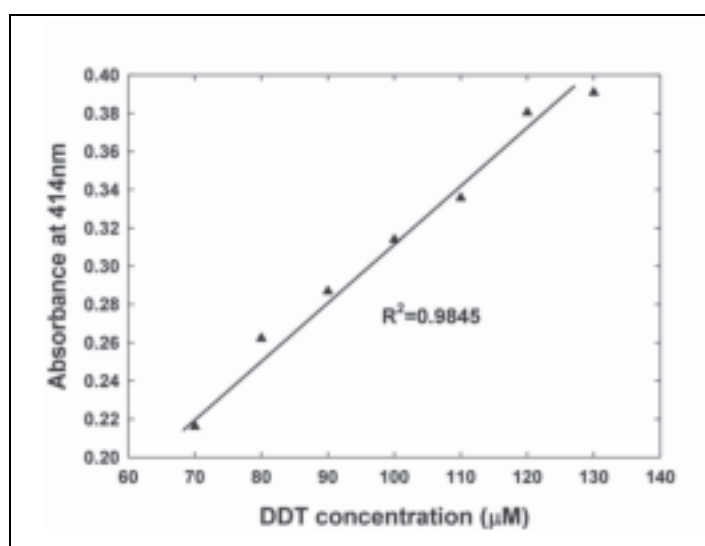


Figure 5.1. Dithiothreitol (DTT) calibration curve. Each value is an average of triplicate determinations with a percentage relative standard deviation of less than 5%.

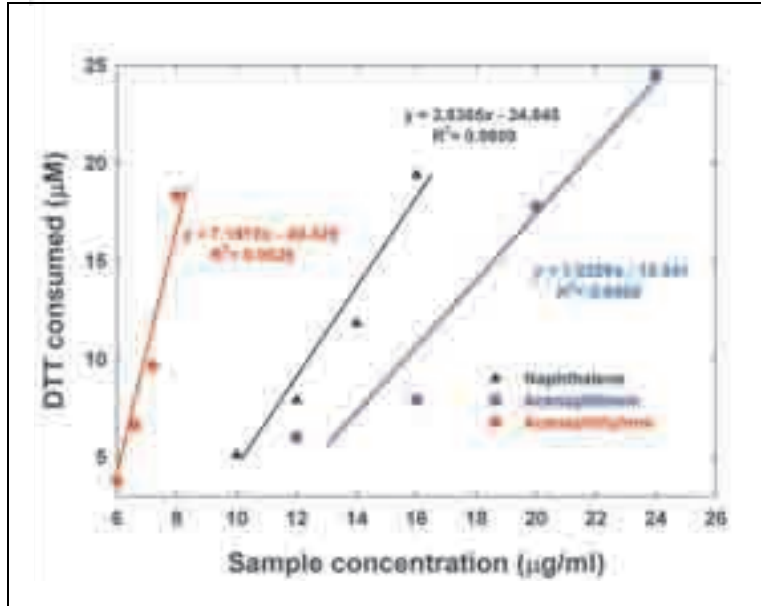


Figure 5.2. Dithiothreitol (DTT) consumption by secondary organic aerosol generated from the photooxidation of three polycyclic aromatic hydrocarbons.

the fact that acenaphthene produced the lowest response is consistent with the finding that no quinones were observed as products from the photooxidation of this compound. It has to be noted

that the DTT assay was applied to only one filter sample for each reaction. As a result, the reproducibility of the results needs to be further investigated.

6 Conclusions and Recommendations

A detailed programme of laboratory experiments was performed on the atmospheric degradation of naphthalene. The yields of SOA formed from the gas-phase reaction of naphthalene with the OH radical were found to be dependent on the concentrations of naphthalene and NO_x as well as on the RH, being higher with higher hydrocarbon (HC)/ NO_x and higher RH. The higher SOA yields with higher HC/ NO_x could be attributed to RO_2 - NO_x chemistry as discussed above. However, the reason for the higher SOA yields at higher RH remains unclear and further investigations into the effects of RH on the SOA yields are therefore needed.

The gas- and particle-phase atmospheric oxidation products of naphthalene were identified using GC-MS. A series of carbonyls and hydroxylated compounds were identified. However, many of these products are not commercially available and quantification is thus problematic. Aerosol Time-of-Flight Mass Spectrometry was utilised to analyse the composition of SOA in real time, providing useful information on the composition and formation mechanisms of SOA from atmospheric degradation of naphthalene. Further experiments are recommended to investigate the SOA chemical composition under different initial conditions, e.g. presence/absence of NO_x and different RH values.

A series of experiments was also performed on two other PAHs, acenaphthene and acenaphthylene. Rate coefficients for the reaction of these compounds with OH radicals, NO_3 radicals and O_3 were measured and used to calculate atmospheric lifetimes. The results suggest that acenaphthene and acenaphthylene will react within a few hours of being released into the atmosphere and therefore contribute to local air pollution. Detailed studies on the OH-radical-initiated oxidation of acenaphthene and acenaphthylene were performed and the gas- and particle- phase products were determined. Reaction mechanisms for the atmospheric degradation of acenaphthene and acenaphthylene were proposed. Further investigations on the products and mechanisms for the reactions with the NO_3 radical and O_3 are recommended.

Experiments were also performed to assess the relative toxicity of SOA formed from the atmospheric degradation of naphthalene, acenaphthene and acenaphthylene. A preliminary study involving the use of a biochemical (DTT) assay showed that the SOA from acenaphthylene and acenaphthene produced the highest and lowest amounts of ROS, respectively. Further tests, including those using cell-based assays, are required to investigate the reproducibility of the experiments and the possible correlation of quinone concentrations with toxicity.

References

- Annathula, R., Yamada, T. and Taylor, P., 2007. Kinetics of OH radical reaction with phenanthrene: New absolute rate measurements and comparison with other PAHs. *International Journal of Chemical Kinetics* **39**: 629–637.
- Atkinson, R. and Arey, J., 1994. Atmospheric chemistry of gas-phase polycyclic aromatic hydrocarbons: formation of atmospheric mutagens. *Environmental Health Perspectives* **102**(4): 117–126.
- Atkinson, R. and Arey, J., 2003. Atmospheric degradation of volatile organic compounds. *Chemical Reviews* **103**: 4605–4638.
- Atkinson, R. and Arey, J., 2007. Mechanisms of the gas-phase reactions of aromatic hydrocarbons and PAHs with OH and NO₃ radicals. *Polycyclic Aromatic Compounds* **27**: 15–40.
- Atkinson, R. and Aschmann, S.M., 1988. Kinetics of the reactions of acenaphthene and acenaphthylene and structurally-related aromatic compounds with OH and NO₃ radicals, N₂O₅ and O₃ at 296 ± 2 K. *International Journal of Chemical Kinetics* **20**: 513–539.
- Atkinson, R., Arey, J., Zielinska, B. and Aschmann, S.M., 1987. Kinetic and products of the gas-phase of OH radicals and N₂O₅ with naphthalene and biphenyl. *Environmental Science & Technology* **21**: 1014–1022.
- Baltensperger, U., Kalberer, M., Dommen, J., Paulsen, D., Alfarra, M.R., Coe, H., Fisseha, R., Gascho, A., Gysel, M., Nyeki, S., Sax, M., Steinbacher, M., Prevot, A.S.H., Sjögren, S., Weingartner, E. and Zenobi, R., 2005. Secondary organic aerosol from anthropogenic and biogenic precursors. *Faraday Discussions* **130**: 265–278.
- Banceu, C.E., Mihele, C., Lane, D.A. and Bunce, N.J., 2001. Reactions of methylated naphthalenes with hydroxyl radicals under simulated atmospheric conditions. *Polycyclic Aromatic Compounds* **18**: 415–425.
- Bernhard, M.J. and Simonich, S.L., 2000. Use of a bench-top photochemical reactor and solid-phase microextraction to measure semivolatile organic compound-hydroxyl radical rate constants. *Environmental Toxicology and Chemistry* **19**: 1705–1710.
- Biermann, H.W., MacLeod, H., Atkinson, R., Winer, A.M. and Pitts, J.N., Jr., 1985. Kinetics of the gas-phase reactions of the hydroxyl radical with naphthalene, phenanthrene, and anthracene. *Environmental Science & Technology* **19**: 244–248.
- Bolton, J.L., Trush, M.A., Penning, T.M., Dryhurst, G. and Monks, T.J., 2000. Role of quinines in toxicology. *Chemical Research in Toxicology* **13**: 135–160.
- Brubaker, W.W., Jr. and Hites, R.A., 1998. OH reaction kinetics of polycyclic aromatic hydrocarbons and polychlorinated dibenzo-p-dioxins and dibenzofurans. *The Journal of Physical Chemistry A* **102**: 915–921.
- Bunce, N.J., Liu, L., Zhu, J. and Lane, D.A., 1997. Reaction of naphthalene and its derivatives with hydroxyl radicals in the gas phase. *Environmental Science & Technology* **31**: 2252–2259.
- Calvert, J.G., Atkinson, R., Becker, K.H., Kamens, R.M., Seinfeld, J.H., Wallington, T.J. and Yarwood, G., 2002. *The Mechanisms of Atmospheric Oxidation of Aromatic Hydrocarbons*. Oxford University Press, Oxford, UK.
- Chan, A.W.H., Kautzman, K.E., Chhabra, P.S., Surratt, J.D., Chan, M.N., Crouse, J.D., Kürten, A., Wennberg, P.O., Flagan, R.C. and Seinfeld, J.H., 2009. Secondary organic aerosol formation from photooxidation of naphthalene and alkylnaphthalenes: implications for oxidation of intermediate volatility organic compounds (IVOCs). *Atmospheric Chemistry and Physics Discussions* **9**: 1873–1905.
- Cho, A.K., Stefano, E.D., You, Y., Rodriguez, C.E., Schmitz, D.A., Kumagai, Y., Miguel, A.H., Eiguren-Fernandez, A., Kobayashi, T., Avol, E. and Froines, J.R., 2004. Determination of four quinines in diesel exhaust particles, SRM 1649a, and atmospheric PM_{2.5}. *Aerosol Science and Technology* **38**: 68–81.
- Cocker, D.R., Mader, B.T., Kalberer, M., Flagan, R.C. and Seinfeld, J.H., 2001. The Effect of water on gas-particle partitioning of secondary organic aerosol. Part 2. m-xylene and 1,3,5-trimethylbenzene photooxidation systems. *Atmospheric Environment* **35**: 6073–6085.
- Cousins, I.T. and Mackay, D., 2001. A critical review of gas-particle partitioning of organic compounds and its interpretation using relative solubilities. *Environmental Science & Technology* **35**: 643–647.
- Dockery, D.W., Pope, C.A., Xu, X., Spengler, J.D., Ware, J.H., Fay, M.E., Ferris, B.G. and Speizer, F.E., 1993. An association between air pollution and mortality in six U.S. cities. *New England Journal of Medicine* **329**: 1753–1759.
- Edney, E.O., Driscoll, D.J., Speer, R.E., Weathers, W.S., Kleindienst, T.E., Li, W. and Smith, D.F., 2000. Impact of aerosol liquid water on secondary organic aerosol

- yields of irradiated toluene/propylene/NOx/(NH₄)₂SO₄/air mixture. *Atmospheric Environment* **34**: 3907–3919.
- Finlayson-Pitts, B.J., Wingen, L.M., Sumner, A.L., Syomin, D. and Ramazan, K.A., 2003. The heterogeneous hydrolysis of NO₂ in laboratory systems and in outdoor and indoor atmospheres: an integrated mechanism. *Physical Chemistry Chemical Physics* **5**: 223–242.
- Finlayson-Pitts, B.J. and Pitts, J.N., 2000. *Chemistry of the Upper and Lower Atmosphere*. Academic Press, San Diego, USA.
- Gross, D.S., Gaelli, M.E., Kalberer, M., Prevot, A.S., Dommen, J., Alfarra, M.R., Duplissy, J., Gaeggeler, K., Gascho, A., Metzger, A. and Baltensperger, U., 2006. Real-time measurement of oligomeric species in secondary organic aerosol with the aerosol time-of-flight mass spectrometer. *Analytical Chemistry* **78**: 2130–2137.
- Healy, R.M., Wenger, J.C., Metzger, A., Duplissy, J., Kalberer, M. and Dommen, J., 2008. Gas/particle partitioning of carbonyls in the photooxidation of isoprene and 1,3,5-trimethylbenzene. *Atmospheric Chemistry and Physics* **8**: 3215–3230.
- Healy, R.M., Temime, B., Kuprovskite, K. and Wenger, J.C., 2009. Effect of relative humidity on gas/particle partitioning and aerosol mass yield in the photooxidation of p-xylene. *Environmental Science & Technology* **43**: 1884–1889.
- Henry, F., Coeur-Tourneur, C., Ledoux, F., Tomas, A. and Menu, D., 2008. Secondary organic aerosol formation from the gas phase reaction of hydroxyl radicals with *m*-, *o*- and *p*-cresol. *Atmospheric Environment* **42**: 3035–3045.
- Hurley, M.D., Sokolov, O., Wallington, T.J., Takekawa, M., Klotz, B., Barnes, I. and Becker, K.H., 2001. Organic aerosol formation during the atmospheric degradation of toluene. *Environmental Science & Technology* **35**: 1358–1366.
- Johnson, D., Jenkin, M.E., Wirtz, K. and Martin-Reviejo, M., 2004. Simulating the formation of secondary organic aerosol from photooxidation of toluene. *Environmental Chemistry* **1**: 150–165.
- Johnson, D., Jenkin, M.E., Wirtz, K. and Martin-Reviejo, M., 2005. Simulating the formation of SOA from the photooxidation of aromatic hydrocarbons. *Environmental Chemistry* **2**: 35–48.
- Kleindienst, T.E., Smith, D.F., Li, W., Edney, E.O., Driscoll, D.J., Speer, R.E. and Weathers, W.S., 1999. Secondary organic aerosol formation from the oxidation of aromatic hydrocarbons in the presence of dry submicron ammonium sulfate aerosol. *Atmospheric Environment* **33**: 3669–3681.
- Klöpffer, V.W., Frank, R., Kohl, E.-G. and Haag, F., 1986. Quantitative erfassung der photochemischen transformations prozeesse in der troposphere. *Chemiker-Zeitung* **110**: 57–62.
- Kwok, E.S.C., Harger, W.P., Arey, J., Atkinson, R., 1994. Reactions of gas-phase phenanthrene under simulated atmospheric conditions. *Environmental Science & Technology* **28**: 521–527.
- Lee, S., Stevens, P.S. and Hites, R.A., 2003. Rate constants for the gas-phase reactions of methylphenanthrenes with OH as a function of temperature. *The Journal of Physical Chemistry A* **107**: 6603–6608.
- Li, N., Sioutas, C., Cho, A., Schmitz, D.A. and Nel, A., 2003. Ultrafine particulate pollutants induce oxidative stress and mitochondrial damage. *Environmental Health Perspectives* **111**: 455–460.
- Logan, J.A., 1985. Tropospheric ozone: seasonal behavior, trends, and anthropogenic influences. *Journal of Geophysical Research* **90**: 10463–10482.
- Metzger, A., Dommen, J., Gaeggeler, K., Duplissy, J., Prevot, A.S.H., Kleffmann, J., Elshorbany, Y., Wisthaler, A. and Baltensperger, U., 2008. Evaluation of 1,3,5 trimethylbenzene degradation in the detailed tropospheric chemistry mechanism, MCMv3.1, using environmental chamber data. *Atmospheric Chemistry and Physics* **8**: 6453–6468.
- Ng, N.L., Kroll, J.H., Chan, A.W.H., Chhabra, P., Flagan, R.C. and Seinfeld, J.H., 2007. Secondary organic aerosol formation from *m*-xylene, toluene, and benzene. *Atmospheric Chemistry and Physics* **7**: 3909–3922.
- Nishino, N., Atkinson, R. and Arey, J., 2008. Formation of nitro products from the gas-phase OH radical-initiated reactions of toluene, naphthalene, and biphenyl: effect of NO₂ concentration. *Environmental Science & Technology* **42**: 9203–9209.
- Odum, J.R., Hoffmann, T., Bowman, F., Collins, D., Flagan, R.C. and Seinfeld, J.H., 1996. Gas/particle partitioning and secondary organic aerosol yields. *Environmental Science & Technology* **30**: 2580–2585.
- Odum, J.R., Jungkamp, T.P.W., Griffin, R.J., Forstner, H.J.L., Flagan, R.C. and Seinfeld, J.H., 1997. Aromatic, reformulated gasoline, and atmospheric organic aerosol formation. *Environmental Science & Technology* **31**: 1890–1897.
- Platt, U. and Heintz F., 1994. Nitrate radicals in tropospheric chemistry. *Israel Journal of Chemistry* **34**: 289–300.
- Prinn, R.G., Weiss, R.F., Miller, B.R., Huang, J., Alyea, F.N., Cunnold, D.M., Fraser, P.J., Hartley, D.E. and Simmonds, P.G., 1995. Atmospheric trends and lifetime of CH₃CCl₃ and global OH concentrations. *Science* **269**: 187–192.

- Reisen, F. and Arey, J., 2002. Reactions of hydroxyl radicals and ozone with acenaphthene and acenaphthylene. *Environmental Science & Technology* **36**: 4302–4311.
- Rohrer, F., Bohn, B., Brauers, T., Bruning, D., Johnen, F.J., Wahner, A. and Kleffmann, J., 2005. Characterisation of the photolytic HONO-source in the atmosphere simulation chamber SAPHIR. *Atmospheric Chemistry and Physics* **5**: 2189–2201.
- Sasaki, J., Aschmann, S.M., Atkinson, R. and Arey, J., 1997. Products of the gas-phase OH and NO₃ radical-initiated reactions of naphthalene. *Environmental Science & Technology* **31**: 3173–3179.
- Song, C., Na, K. and Cocker, D.R., 2005. Impact of the hydrocarbon to NO_x ratio on secondary organic aerosol formation. *Environmental Science & Technology* **39**: 3143–3149.
- Song, C., Na, K., Warren, B., Malloy, Q. and Cocker, D.R., 2007. Secondary organic aerosol formation from the photooxidation of p- and o-xylene. *Environmental Science & Technology* **41**: 7403–7408.
- Song, C., Na, K., Warren, B., Malloy, Q. and Cocker, D.R., 2007. Secondary organic aerosol formation from m-xylene in the absence of NO_x. *Environmental Science & Technology* **41**: 7409–7416.
- Srogi, K., 2007. Modelling of environmental exposure to polycyclic aromatic hydrocarbons: a review. *Environmental Chemistry Letters* **5**: 169–195.
- Temime, B., Healy, R.M. and Wenger, J.C., 2007. A denuder-filter sampling technique for the detection of gas and particle phase carbonyl compounds. *Environmental Science & Technology* **41**: 6514–6520.
- Wang, L., Arey, J. and Atkinson, R. 2006. Kinetics and products of photolysis and reaction with OH radicals of a series of aromatic carbonyl compounds. *Environmental Science & Technology* **40**: 5465–5471.
- Wang, L., Atkinson, R. and Arey, J., 2007a. Dicarbonyl products of the OH radical-initiated reactions of naphthalene and C1- and C2-alkylnaphthalenes. *Environmental Science & Technology* **41**: 2803–2810.
- Wang, L., Atkinson, R. and Arey, J., 2007b. Formation of 9,10-phenanthrenequinone by atmospheric gas-phase reactions of phenanthrene. *Atmospheric Environment* **41**: 2025–2035.
- Warren, B., Song, C. and Cocker, D.R., 2008. Light intensity and light source influence on secondary organic aerosol formation for the m-xylene/NO_x photooxidation system. *Environmental Science & Technology* **42**: 5461–5466.

Acronyms

API	Atmospheric pressure ionisation
ATOFMS	Aerosol Time-of-Flight Mass Spectrometer
BSTFA	<i>N,O</i> -Bis(trimethylsilyl)trifluoro acetamide
-C(O)	Carbonyl group
CI	Chemical ionisation
DMSO	Dimethyl sulfoxide
DTNB	5,5'-Dithio-bis-2-nitrobenzoic acid
DTT	Dithiothreitol
EI	Electron ionisation
EPA	Environmental Protection Agency
FEP	Fluorine-ethene-propene
FID	Flame ionisation detector
GC-MS	Gas chromatogram-mass spectrometry
HONO	Nitrous acid
MCT	Mercury-cadmium-tellurium
NADH	Nicotinamide adenine dinucleotide
NADPH	Nicotinamide adenine dinucleotide phosphate
NaNO₂	Sodium nitrite
NO	Nitric oxide
NO_x	Nitrogen oxides
O₃	Ozone
OH	Hydroxyl radical
PAH	Polycyclic aromatic hydrocarbon
PFBHA	<i>O</i> -(2,3,4,5,6-pentafluorobenzyl)-hydroxylamine
PM	Particulate matter
ppbV	Parts per billion
PTFE	Polytetrafluoroethylene
RH	Relative humidity
ROS	Reactive oxygen species
SMPS	Scanning mobility particle sizer
SOA	Secondary organic aerosol
UV	Ultraviolet

An Gníomhaireacht um Chaomhnú Comhshaoil

Is í an Gníomhaireacht um Chaomhnú Comhshaoil (EPA) comhlachta reachtúil a chosnaíonn an comhshaoil do mhuintir na tíre go léir. Rialaímid agus déanaimid maoirsiú ar gníomhaíochtaí a d'fhéadfadh truailliú a chruthú murach sin. Cinntímid go bhfuil eolas cruinn ann ar threochtaí comhshaoil ionas go nglactar aon chéim is gá. Is iad na príomh-nithe a bhfuilimid gníomhach leo ná comhshaoil na hÉireann a chosaint agus cinntiú go bhfuil forbairt inbhuanaithe.

Is comhlacht poiblí neamhspleách í an Gníomhaireacht um Chaomhnú Comhshaoil (EPA) a bunaíodh i mí Iúil 1993 faoin Acht fán nGníomhaireacht um Chaomhnú Comhshaoil 1992. Ó thaobh an Rialtais, is í an Roinn Comhshaoil agus Rialtais Áitiúil a dhéanann urraíocht uirthi.

ÁR bhFREAGRACHTAÍ

CEADÚNÚ

Bíonn ceadúnais á n-eisiúint againn i gcomhair na nithe seo a leanas chun a chinntiú nach mbíonn astuithe uathu ag cur sláinte an phobail ná an comhshaoil i mbaol:

- áiseanna dramhaíola (m.sh., líonadh talún, loisceoirí, stáisiúin aistrithe dramhaíola);
- gníomhaíochtaí tionsclaíocha ar scála mór (m.sh., déantúsaíocht cógaisíochta, déantúsaíocht stroighne, stáisiúin chumhachta);
- diantalmhaíocht;
- úsáid faoi shrian agus scaoileadh smachtaithe Orgánach Géinathraithe (GMO);
- mór-áiseanna stórais peitreal.
- Scardadh dramhúisce

FEIDHMIÚ COMHSHAOIL NÁISIÚNTA

- Stiúradh os cionn 2,000 iniúchadh agus cigireacht de áiseanna a fuair ceadúnas ón nGníomhaireacht gach bliain.
- Maoirsiú freagrachtaí cosanta comhshaoil údarás áitiúla thar sé earnáil - aer, fuaim, dramhaíl, dramhúisce agus caighdeán uisce.
- Obair le húdaráis áitiúla agus leis na Gardaí chun stop a chur le gníomhaíocht mhídhleathach dramhaíola trí chomhordú a dhéanamh ar líonra forfheidhmithe náisiúnta, díriú isteach ar chiontóirí, stiúradh fiosrúcháin agus maoirsiú leigheas na bhfadhbanna.
- An dlí a chur orthu siúd a bhriseann dlí comhshaoil agus a dhéanann dochar don chomhshaoil mar thoradh ar a gníomhaíochtaí.

MONATÓIREACHT, ANAILÍS AGUS TUAIRISCIÚ AR AN GCOMHSHAOIL

- Monatóireacht ar chaighdeán aer agus caighdeán aibhneacha, locha, uisce taoide agus uisce talaimh; leibhéil agus sruth aibhneacha a thomhas.
- Tuairisciú neamhspleách chun cabhrú le rialtais náisiúnta agus áitiúla cinntiú a dhéanamh.

RIALÚ ASTUITHE GÁIS CEAPTHA TEASA NA HÉIREANN

- Cainníochtú astuithe gáis ceaptha teasa na hÉireann i gcomhthéacs ár dtiomantas Kyoto.
- Cur i bhfeidhm na Treorach um Thrádáil Astuithe, a bhfuil baint aige le hos cionn 100 cuideachta atá ina mór-ghineadóirí dé-ocsaíd charbóin in Éirinn.

TAIGHDE AGUS FORBAIRT COMHSHAOIL

- Taighde ar shaincheisteanna comhshaoil a chomhordú (cosúil le caighdeán aer agus uisce, athrú aeráide, bithéagsúlacht, teicneolaíochtaí comhshaoil).

MEASÚNÚ STRAITÉISEACH COMHSHAOIL

- Ag déanamh measúnú ar thionchar phleananna agus chláracha ar chomhshaoil na hÉireann (cosúil le plannanna bainistíochta dramhaíola agus forbartha).

PLEANÁIL, OIDEACHAS AGUS TREOIR CHOMHSHAOIL

- Treoir a thabhairt don phobal agus do thionscal ar cheisteanna comhshaoil éagsúla (m.sh., iarratais ar cheadúnais, seachaint dramhaíola agus rialacháin chomhshaoil).
- Eolas níos fearr ar an gcomhshaoil a scaipeadh (trí cláracha teilifíse comhshaoil agus pacáistí acmhainne do bhunscoileanna agus do mheánscoileanna).

BAINISTÍOCHT DRAMHAÍOLA FHORGHNÍOMHACH

- Cur chun cinn seachaint agus laghdú dramhaíola trí chomhordú An Chláir Náisiúnta um Chosc Dramhaíola, lena n-áirítear cur i bhfeidhm na dTionscnamh Freagrachta Táirgeoirí.
- Cur i bhfeidhm Rialachán ar nós na treoracha maidir le Trealamh Leictreach agus Leictreonach Caite agus le Srianadh Substaintí Guaiseacha agus substaintí a dhéanann ídiú ar an gcrios ózóin.
- Plean Náisiúnta Bainistíochta um Dramhaíl Ghuaiseach a fhorbairt chun dramhaíl ghuaiseach a sheachaint agus a bhainistiú.

STRUCHTÚR NA GNÍOMHAIREACHTA

Bunaíodh an Gníomhaireacht i 1993 chun comhshaoil na hÉireann a chosaint. Tá an eagraíocht á bhainistiú ag Bord lánaimseartha, ar a bhfuil Príomhstíúrthóir agus ceithre Stíúrthóir.

Tá obair na Gníomhaireachta ar siúl trí ceithre Oifig:

- An Oifig Aeráide, Ceadúnaithe agus Úsáide Acmhainní
- An Oifig um Fhorfheidhmiúchán Comhshaoil
- An Oifig um Measúnacht Comhshaoil
- An Oifig Cumarsáide agus Seirbhísí Corparáide

Tá Coiste Comhairleach ag an nGníomhaireacht le cabhrú léi. Tá dáréag ball air agus tagann siad le chéile cúpla uair in aghaidh na bliana le plé a dhéanamh ar cheisteanna ar ábhar imní iad agus le comhairle a thabhairt don Bhord.

Science, Technology, Research and Innovation for the Environment (STRIVE) 2007-2013

The Science, Technology, Research and Innovation for the Environment (STRIVE) programme covers the period 2007 to 2013.

The programme comprises three key measures: Sustainable Development, Cleaner Production and Environmental Technologies, and A Healthy Environment; together with two supporting measures: EPA Environmental Research Centre (ERC) and Capacity & Capability Building. The seven principal thematic areas for the programme are Climate Change; Waste, Resource Management and Chemicals; Water Quality and the Aquatic Environment; Air Quality, Atmospheric Deposition and Noise; Impacts on Biodiversity; Soils and Land-use; and Socio-economic Considerations. In addition, other emerging issues will be addressed as the need arises.

The funding for the programme (approximately €100 million) comes from the Environmental Research Sub-Programme of the National Development Plan (NDP), the Inter-Departmental Committee for the Strategy for Science, Technology and Innovation (IDC-SSTI); and EPA core funding and co-funding by economic sectors.

The EPA has a statutory role to co-ordinate environmental research in Ireland and is organising and administering the STRIVE programme on behalf of the Department of the Environment, Heritage and Local Government.